Master's Thesis

Design of an Experiment to Investigate the Λ-n Interaction via the Final State Interaction

Imro'atus Syarifatul Hasanah

Department of Physics
Graduate School of Science
Tohoku University

September, 2017

.

Abstract

The Neutral Kaon Spectrometer 2 (NKS2) collaboration has been studying the strangeness photoproduction in $\gamma + d$ reaction near the threshold [1, 2] at Research Center for ELectron PHoton (ELPH) Tohoku University from 2004. The goal of this experiment is to understand the photoproduction mechanism of neutral kaon and the Λ hyperon from deuteron. NKS2 is a suitable spectrometer to measure the differential cross section of the $\gamma(n, K^0)\Lambda$ channel because NKS2 can detect charged particles from K^0 and Λ decays effectively thanks to its large solid angle ($\Omega \simeq \pi$sr).

For the first time after the East Japan earthquake, we started physics experiments from 2016. Our motivation to measure η production is to calibrate the absolute photon energy by using the threshold energy. A production experiment for η meson was performed on February with liquid hydrogen target ($\gamma p \to p$). A cross section measurement for Λ hyperon was performed in June with liquid deuterium target ($\gamma d \to K^0\Lambda$). We succeeded to take physics data in these experiments.

The current status of NKS2, kaon identification is still not good enough for a mass square spectrum because time resolution of hodoscopes is not enough to separate kaon, pion, and proton clearly. Thus we wish to enhance NKS2 Time-of-Flight (TOF) resolution to separate kaon from other particles. A typical time resolution (σ) of hodoscopes was about 400 ps, which was sufficient to separate pions and protons in a momentum range less than 800 MeV/c. By using Multi-gap Resistive Plate Chamber (MRPC), we expect that it can improve the NKS2 TOF resolution to less than $\sigma \sim$100 ps (so that it is easy to identify kaon) and measure the Λ-n interaction in $\gamma d \to K^+\Lambda n$. In this thesis, I design an experiment to study the Λ-n

interaction via Final State Interaction (FSI) with the GEANT4 simulation in order to check the feasibility of the Λ-n FSI experiment with NKS2.

A new future experiment focuses on now investigating Λ-n interaction via a K^+ measurement in γd reaction. Recent experimental progresses on ${}^{4}_{\Lambda}$H and ${}^{4}_{\Lambda}$He revealed the importance of the charge symmetry breaking (CSB) in the ΛN interaction.

One of the keys to understanding the Λ-N CSB is a comparison of Λp with Λn interaction by direct measurement. However, a direct scattering measurement is so difficult. There are no data about Λ-n scattering. We need indirect scattering measurement. To obtain information about the Λ-n interaction, we propose a different kind of experiment from hypernuclear studies which require not only details about the interaction but also detailed discussions on nuclear structure. Our motivation is to define and measure the scattering length and effective range of the Λ-n interaction via a K^+ measurement in γd reaction.

To obtain a FSI enhancement factor, we adopted the Watson-Migdal approximation [3, 4]. The enhancement factor becomes larger in lower relative momentum region. It is unclear how the lower relative momentum region is related in the K^+ and/or K^+ Λ measurement as a function of momentum, angle, and cross section.

From the simulation result, we can see the enhancement factors by Λ-n FSI effect are larger in lower E_γ region (800-900 MeV), but still remain higher region. In the low relative momentum region, events are located in the forward angle region of K^+ not limited to zero degree. It suggests that a wide coverage of the acceptance is necessary to measure the FSI enhancement effect, which can be measured by the NKS2. The geometry acceptance for K^+ single measurement with 2 charged-particle trigger has been estimated as about 20% for all events by the GEANT4 simulation. The K^0_S acceptance was as about 1% order. Using scaling of acceptance and data analyzed previously taken with NKS2, we predict that 180 to 18 shifts (90 to 9 days) are required to obtain $30\times10^3 K^+$'s to have 1% precision of the K^+ yield. It will allow us to discriminate models.

Acknowledgements

My sincerest thanks are experessed to my supervisor, Prof. Satoshi N. Nakamura, for his teaching and guidance to me during my two years study. His professionality and broad knowIedge always encourage me to study more and more about physics.

I must specifically thank to Dr. Masashi Kaneta for dedicating his precious time to help and guide me during my study.

I am very grateful to Dr. Sho Nagao and Dr. Toshiyuki Gogami for always allocating time for me to have discussion every time I encounter some problems in my research.

I would like to specially thank Prof. Hirokazu Tamura and Prof. Takeshi Koike to allocating many time many times to study more in the Hypernuclear meeting and seminar.

I am sincerely thankful to NKS2 group from Intermediate Nuclear Physics, Prof. Kazushige Maeda and Prof. Hiroki Kanda. They were always willing and able to provide me with his patience and guidance. Aki Ninomiya, who always help me to solve my problem about some courses and learn for experiment.

I am grateful to all of staff of Hypernuclear Physics group. Mrs. Yoko Wada and Mrs. Yumi Suzuki, who always handle my of my administration very patiently, deftly, and kindly. Mr. Hiroki Umezu who always handle of technical issues in the experiment.

To the past and present students of Hypernuclear Physics group, I am thankful to Takeshi Yamamoto, Sasaki Yuki, Yuya Akazawa, Manami Fujita, Sadami Suto, Yuta Takahashi, Yuichi Toyama, M. Ikeda, Yuu Ogura, Aida Genki, Sachitaro Ozawa, Honoka Kanauchi, Hiroki Takeuchi, Yuta

Muroi, Yuji Ishikawa, Hiroshi Itabashi, Yoshihiro Konishi, Norina Fujioka. I am forever indebted for your endless patience have been willing to try communicate in English with me, so very help me further my education. I am also very grateful to my tutors, Shoko Tomita, for her helps on many things and kindness to me during my study.

This study was possible due to the funding provided though MEXT Scholarship, IGPAS program and fellowship. Special thanks is extended to Mrs. Mika Kikuchi and Mrs. Michiko Kohama of the DIRECT department. Prima Wira Kusuma Wardhani, Irwan, Seno Aji, M Riza Iskandar, Theodorus Permana, Yan Fahmi Swastiraras, Annisa Noorhidayati and Layli Amaliya, Indonesian friends who passed in the IGPAS program.

As a muslim, I want to thanks a lot to Allah Almighty God, the most gracious and the most merciful, for His blessing in completing this thesis. Alhamdulillah, all praises to Allah, to whom I pray and seeking for strengths in my difficult times.

The last, but not least, I want to give my best thanks to my mother, my husband and my baby boy for your supports and a lot prayers for me.

Imroatus Syarifatul Hasanah

Tohoku University

Contents

List of Figures

List of Tables

1

Introduction

1.1 Overview and Structure of Thesis

The reaction of interest discussed in this thesis is the $\Lambda - n$ interaction via a K^+ measurement in $\gamma - d$ reaction. The first chapter will briefly review the current description of hyperon and history of strangeness physics including the nuclear structure and baryon interaction. This chapter will discuss the importance of Baryon-Baryon (BB) interaction and how to define the BB interaction from experimental data. It will then discusses existing experimental method to study the $\Lambda - N$ interaction, present the motivation for studying this reaction, the relevance of its study and clearly identifies the aim of this particular study. The second chapter explains the principle of the experiment to review existing theoretical estimations like scattering lengths and effective ranges, enhancement factor, and the missing mass. It will then discuss the theoretical calculation. The third chapter is concerned with existing experimental apparatus such as the experimental hall, beam line and detectors. It will also discuss about the improvement of experimental design. The fourth chapter shall expound upon the upgrade plan, set up in the GEANT4 Simulation, expected result and also expected $\Lambda - n$ interaction. The last chapter is summary and discussion.

1.2 Hyperon

Hyperon is a baryon containing one or more strange quarks. Being baryons, all hyperons are fermions. That is, they have half-integer spin and obey Fermi-Dirac statistics. They all interact via the strong nuclear force making them types of hadron. They are

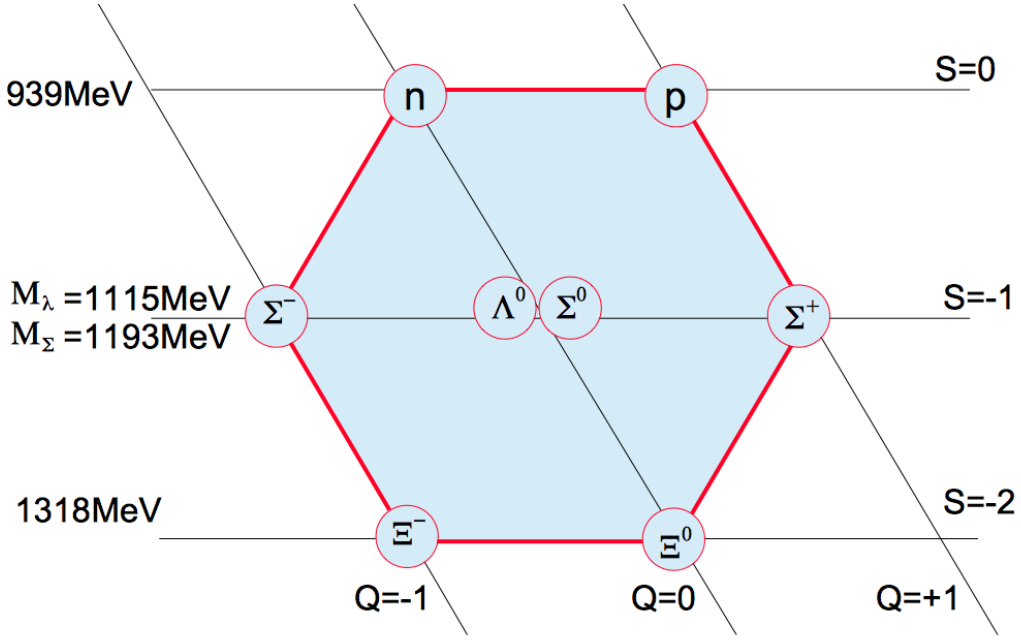

Figure 1.1: Ground state hyperon, spin 1/2, with strangeness S and charge Q.

composed of three light quarks, at least one of which is a strange quark, which makes them strange baryon.

Since strangeness is conserved by the strong interactions, the ground-state hyperons (spin 1/2) as shown in Figure 1.1 cannot decay via strong interaction. For more detail description, see section 1.3.2.

1.3 History of Strangeness Physics

1.3.1 Nuclear Structure

The structure of matter and the interactions among its constituents at the nuclear scale are the focus of research conducted by a nuclear physicist. The motivation to conduct nuclear experiments lie deep in the rich and complex structure of the nuclei, the fundamental forces which serve to hold together the natural order is still not fully understood. Moreover, the nucleon is one of the subatomic particles that constitute the nucleus [6]. By studying the nucleus and the forces that play a dominant role on the scale, we can determine the strength of the interaction. Nucleon is not a point particle

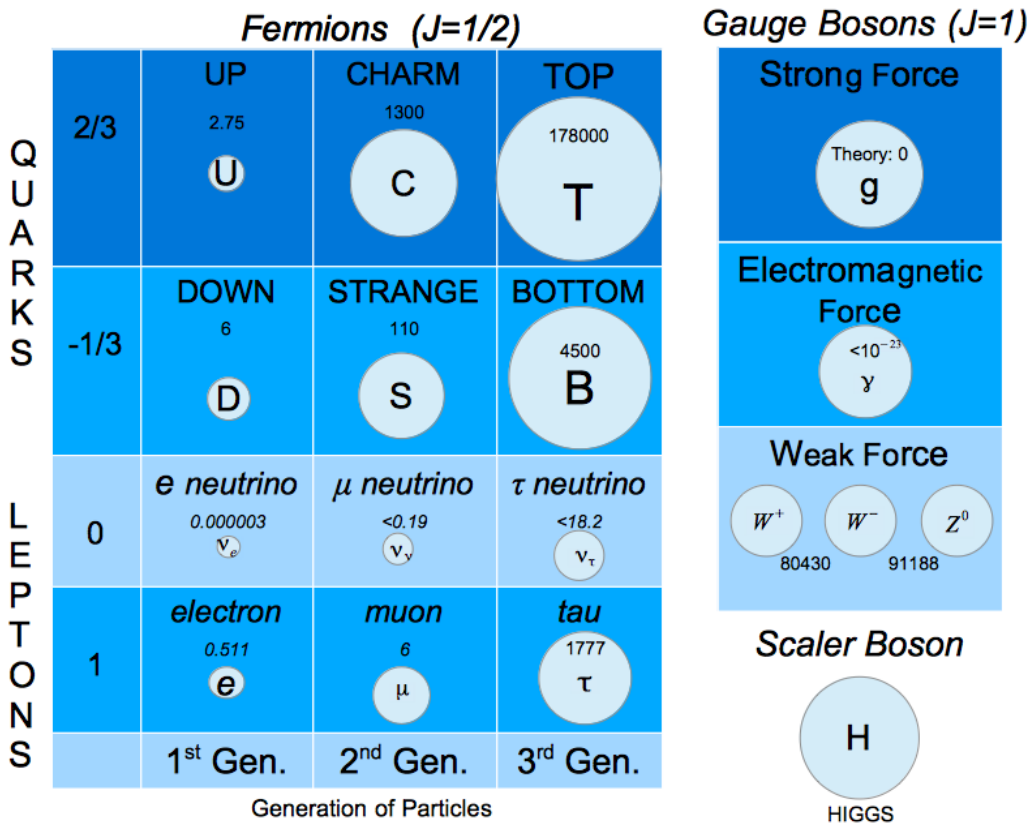

Figure 1.2: The contemporary description of subatomic particles and forces is called the standard model. The values on each panel represent of the mass of paticles.

but a composite structure complex and our understanding of one of the basic forces of nature is still far from complete.

The matter is made up of particles that carry the intrinsic spin of 1/2 and called fermions, which include two types of particles that are believed to have no further internal structure, so it can be considered as a point. Quarks and leptons are called point-like particles without structure. All interactions are considered being mediated by particles in the standard models, as shown in Figure 1.2.

The standard model states that the interaction is achieved through the exchange of particles called as gauge bosons. The weak interaction is mediated by three different particles, and at this point there is no short quantization of gravity. All the materials are assembled from a combination of quarks which are defined as hadrons and held together by the strong force.

Currently, the nucleon is a baryon and has the lowest mass, which can be categorized into proton (uud) and the neutron (udd). Quark and anti-quark form a meson, which at the nuclear level is the mediator of the strong nuclear force predicted by Yukawa [7].

1.3.2 Baryon Interaction

If three quarks (each with spin 1/2) are to yield a spin 1/2 baryon, then the spin of one of the quarks must be antiparallel to the other two. This is not possible for the uuu, ddd and sss quark combinations. There are then only two different possible combinations of u and d quarks which can fulfil the necessary symmetry conditions on the wave function of a spin 1/2 baryon, and these are just the proton and the neutron. The proton and neutron wave functions may be schematically written as:

$$\begin{aligned} |p^{\uparrow}\rangle &= |u^{\uparrow}u^{\uparrow}d^{\downarrow}\rangle \\ |n^{\uparrow}\rangle &= |u^{\downarrow}d^{\uparrow}d^{\uparrow}\rangle \end{aligned} \tag{1.3.1}$$

For a proton with, the z spin component m_J =+1/2, we may write the spin wave function as a product of the spin wave function of one quark and that of the remaining pair:

$$\chi_p(J=1/2, m_J=1/2) = \sqrt{2/3}\chi_{uu}(1,1)\chi_d(1/2,-1/2) - \sqrt{1/3}\chi_{uu}(1,0)\chi_d(1/2,1/2). \tag{1.3.2}$$

The factors in this equation are the Clebsch-Gordan coefficients, to single out the d-quark and coupled the u-quark pair, for the coupling of spin 1 and spin 1/2. Replacing $\chi(1,\ 0)$ by the correct spin triplet wave function $(\uparrow\downarrow\ +\ \downarrow\uparrow)/\sqrt{2}$ then yields in our spin-flavour notation

$$|p^{\uparrow}\rangle = \sqrt{2/3}|u^{\uparrow}u^{\uparrow}d^{\downarrow}\rangle - \sqrt{1/6}|u^{\uparrow}u^{\downarrow}d^{\uparrow}\rangle - \sqrt{1/6}|u^{\downarrow}u^{\uparrow}d^{\uparrow}\rangle. \tag{1.3.3}$$

This expression is still only symmetric in terms of the exchange of the first and second quarks, and not for two quarks. It can, however, be straightforwardly totally symmetrised by swapping the first and third as well as the second and third quarks in each term of this last equation and adding these new terms. With the correct normalisation factor the totally symmetric proton wave function is then

$$\begin{aligned} |p^{\uparrow}\rangle =& \frac{1}{\sqrt{1/18}}\{2|u^{\uparrow}u^{\uparrow}d^{\downarrow}\rangle + 2|u^{\uparrow}d^{\downarrow}u^{\uparrow}\rangle + 2|d^{\downarrow}u^{\uparrow}u^{\uparrow}\rangle - |u^{\uparrow}u^{\downarrow}d^{\uparrow}\rangle - |u^{\uparrow}d^{\uparrow}u^{\downarrow}\rangle - |d^{\uparrow}u^{\uparrow}u^{\downarrow}\rangle \\ & - |u^{\downarrow}u^{\uparrow}d^{\uparrow}\rangle - |u^{\downarrow}d^{\uparrow}u^{\uparrow}\rangle - |d^{\uparrow}u^{\downarrow}u^{\uparrow}\rangle\}. \end{aligned} \tag{1.3.4}$$

The neutron wave function is trivially found by exchanging the u and d quarks:

$$|n^{\uparrow}\rangle = \frac{1}{\sqrt{1/18}}\{2|d^{\uparrow}d^{\uparrow}u^{\downarrow}\rangle + 2|d^{\uparrow}u^{\downarrow}d^{\uparrow}\rangle + 2|u^{\downarrow}d^{\uparrow}d^{\uparrow}\rangle - |d^{\uparrow}d^{\downarrow}u^{\uparrow}\rangle - |d^{\uparrow}u^{\uparrow}d^{\downarrow}\rangle - |u^{\uparrow}d^{\uparrow}d^{\downarrow}\rangle - |d^{\downarrow}d^{\uparrow}u^{\uparrow}\rangle - |d^{\downarrow}u^{\uparrow}d^{\uparrow}\rangle - |u^{\uparrow}d^{\downarrow}d^{\uparrow}\rangle\}. \tag{1.3.5}$$

The nucleons have isospin 1/2 and so form an isospin doublet. A further doublet may be produced by combining two s-quarks with a light quark. This is schematically given by

$$\begin{aligned} |\Xi^{0\uparrow}\rangle &= |u^{\downarrow}s^{\uparrow}s^{\uparrow}\rangle \\ |\Xi^{-\uparrow}\rangle &= |d^{\downarrow}s^{\uparrow}s^{\uparrow}\rangle \end{aligned} \tag{1.3.6}$$

The remaining quark combinations are an isospin triplet and a singlet:

$$\begin{aligned} |\Sigma^{+\uparrow}\rangle &= |u^{\uparrow}u^{\uparrow}s^{\downarrow}\rangle \\ |\Sigma^{0\uparrow}\rangle &= |u^{\uparrow}d^{\uparrow}s^{\downarrow}\rangle \\ |\Sigma^{-\uparrow}\rangle &= |d^{\uparrow}d^{\uparrow}s^{\downarrow}\rangle \\ |\Lambda^{0\uparrow}\rangle &= |u^{\uparrow}d^{\downarrow}s^{\uparrow}\rangle. \end{aligned} \tag{1.3.7}$$

Note that the *uds* quark combination appears twice here and depending upon the relative quark spins and isospins can correspond to two different particles. If the u and d spins and isospins couple to 1, as they do for the charged Σ baryons, then the above quark combination is a Σ^0. If they couple to zero we are dealing with a Λ^0 [7].

1.4 Experimental Method to Study Λ-N Interaction

1.4.1 Charge Symmetry Breaking (CSB) in The Λ-N Interaction

Charge symmetry is defined as the invariance of the strong interaction under an isospin rotation exchanging u and d quarks; it corresponds precisely to a rotation by π about the 2 axis in isospin space (compared to isospin symmetry, which is invariance under an arbitrary rotation in this space) [8]. A new future study includes investigating the Λ-n interaction via a K^+ measurement in γ+d reaction. Most past efforts involving the Λ-N interaction had been studied mainly through light-heavy hypernuclei. Results from these studies have highlighted a discrepancy between experimental data and theoretical calculations of the Λ binding energy of ${}^{4}_{\Lambda}$H and ${}^{4}_{\Lambda}$He. The source of this inconsistency is attributed to the charge symmetry breaking (CSB) in Λ-N interaction. Recent

reporting of precise measurements of ${}^{4}_{\Lambda}$H at MAMI [9] and ${}^{4}_{\Lambda}$He at J-PARC support a large breaking of CSB in the Λ-N interaction.

1.4.2 The Difficulty of Direct Measurement

One of keys for understanding the Λ-N CSB is a comparison of Λ-p with Λ-n interaction by direct measurement. Presently there are no reported data sets for Λ-n scattering primarily due to lack of a neutron targe; in contrast, there have been reported data for Λ-p interaction from scattering experiments. Consequently, the S-wave Λ-n scattering length is still not defined. To obtain information on the Λ-n interaction, we propose a different kind of experiment from hypernuclear studies, which require not only details of the interaction, but also that of nuclear structure. The K^+ measurement of γ+d reaction should yield important information on inelastic scattering and the low energy region of Λ-n interaction.

1.5 Study of Λ-n Interaction via Final State Interaction (FSI)

The principle to extract Λ-n interaction from $\gamma d \to K^+\Lambda n$ is to use indirect measurement. From Figure 1.3, we can identify Λ with $p\pi^-$ invariant mass, then identify K^+. Missing mass (Mx) of $\gamma d \to K^+\Lambda X$ is required to be approximately the mass of the neutron. From that step we can investigate Λ-n interaction via Final State Interaction in γd reaction.

To obtain a FSI enhancement factor, we adopted the Watson-Migdal approximation [3, 4].

$$|C_{FSI}|^2 = \frac{q^2+\beta^2}{q^2+\alpha^2} \tag{1.5.1}$$

The factors described in the equation 1.5.1. are $\alpha = \frac{1}{r}\left(1-\sqrt{1-2\frac{r}{a}}\right)$, $\beta = \frac{1}{r}\left(1+\sqrt{1-2\frac{r}{a}}\right)$. q is a relative momentum of Λ in the Λ-n rest-frame system. The potential parameters, α and β, are described by the scattering lengths a and the effective ranges r of low energy S-wave scattering. To understand the enhancement factor as a function of the Λ-n relative momentum q, we compute the enhancement factor as a function of q by using combination of a and r. The factor increases with smaller relative momentum.

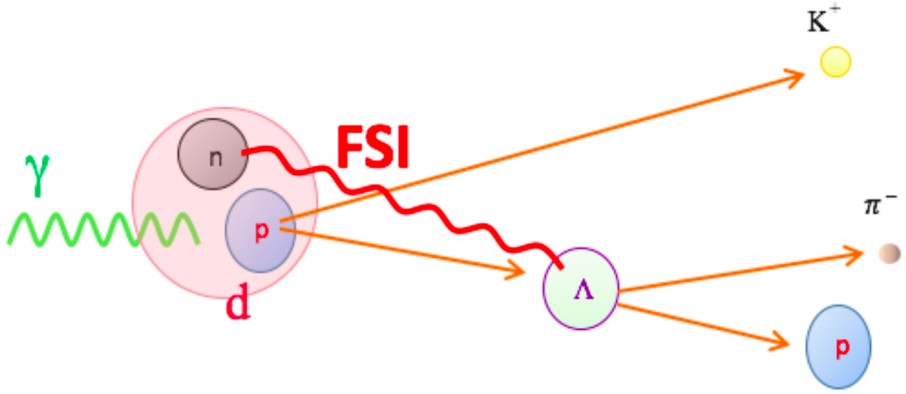

Figure 1.3: Schematic of Λn interaction via FSI in γd reaction

The enhancement shows various dependences and the difference is stronger in spin-singlet state over the triplet state. But the difference became small after the effects from single and triple are added. The enhancement factor became larger in lower relative momentum region. It is unclear how the lower relative momentum region is related in the K^+ and/or K^+ Λ measurement as a function momentum, angle, and cross section. The low relative momentum region is located in the forward angle region of K^+ but not limited to at zero degree. It suggests that a wide coverage of acceptance is necessary to measure the FSI enhancement effect which is possible by the NKS2 (Neutral Kaon Spectrometer 2). The NKS2 was developed to study the photo-production mechanism of K^0 and Λ hyperons in deuteron. By the FSI effect of Λ n, the cross section of K^+ is changed. Its effect appears in K^+ cross section. The FSI of Λ n affects the cross section of K^+ and thus precise measurement of the photoproduction K^+ cross section will give information about the Λ n interaction.

1.6 Physics Motivation

In the current status of NKS2, kaon identification is still very difficult on mass square spectrum because the recent hodoscopes, which are Inner Hososcope (IH) and Outer Hodoscope (OH) time resolution are not enough to separate kaon, pion, and proton. Thus we want to enhance the NKS2 Time of Flight (TOF) resolution to separate kaon from other particles. The typical TOF resolution of IH and OH was the order of 400 ps, which was sufficient to separate pions and protons in a momentum range less than 800

MeV/c. By using Multi-gap Resistive Plate Chamber (MRPC), we expect to improve the NKS2 TOF resolution to less than 100 ps (so that it can identify kaon) and to measure the Λ n interaction in $\gamma d \rightarrow K^{+}\Lambda n$. I am designing an experiment to study the Λ n interaction via Final State Interaction (FSI) with the GEANT4 simulation, from which it is posible to estimate the feasibility of the Λ-n FSI in NKS2.

A new future focus now investigating Λ n interaction via a K^{+} measurement in γd reaction. Most past efforts involving the Λ N interaction had been studied mainly through light-heavy hypernuclei. Results from these studies have highlighted a discrepancy between experimental data and theoretical calculations of the Λ binding energy of ${}^{4}_{\Lambda}$H and ${}^{4}_{\Lambda}$He. The source of this inconsistency is attributed to the charge symmetry breaking (CSB) in the Λ N interaction.

One of the keys in understanding the Λ N CSB is a comparison of Λp with Λn interaction by direct measurement. However, direct scattering measurement is so difficult. There are no data about ΛNn scattering. So, we need indirect scattering measurement. To obtain information about the ΛNn interaction, we propose a different kind of experiment from hypernuclear studies, which requires not only details about the interaction, but also discussions on nuclear structure. So, our motivation is to define and measure the scattering length and effective range of the ΛNn interaction via a K^{+} measurement in γd reaction Figure 1.3.

2

Principle of the Experiment

2.1 Theoretical Estimation

2.1.1 Scattering Lengths and Effective Ranges

Scattering length is a parameter used in analyzing nuclear scattering at low energies. As the energy of the bombarding particle becomes very small, the scattering cross section approaches that of an impenetrable sphere whose radius equals this length [10]. The scattering length appears explicitly in the scattering wave function in the low energy limit. The scattering length is accordingly determined by the position of the node in the linear extrapolation of the radial wave in the limit of zero energy. The effective range formula for scattering by a short range potential is derived for arbitrary angular momentum of the scattered particle [11].

To obtain a FSI enhancement factor, we adopted Watson-Migdal [3, 4]. This factor is described as the following equation

$$|C_{FSI}|^2 = \frac{q^2 + \beta^2}{q^2 + \alpha^2}, \tag{2.1.1}$$

where $\alpha = \frac{1}{r}\left(1 - \sqrt{1 - 2\frac{r}{a}}\right)$, $\beta = \frac{1}{r}\left(1 + \sqrt{1 - 2\frac{r}{a}}\right)$, and q is a relative momentum of Λ in the Λ-n rest-frame system. The potential parameters, α and β, are described by the scattering lengths a and the effective ranges r of low energy S-wave scattering. In this framework we also take into account the spin-singlet ($^1S_0$) and triplet ($^3S_1$) and add those effects coherently. Therefore, the total enhancement factor is described as:

$$\frac{1}{4}|C_{^1S_0 FSI}|^2 + \frac{3}{4}|C_{^3S_1 FSI}|^2. \tag{2.1.2}$$

In order to understand the enhancement factor as a function of the Λ-n relative momentum q, we computed the enhancement factor, by using combination of a and r.

2.1.2 Enhancement Factor

The enhancement shows various dependences and the difference is stronger in spin-singlet state over the triplet state. But, the difference became small after the effects of single and triple were added. The enhancement factor become larger in lower relative momentum region is related in the K^+ and/or $K^+ + \Lambda$ measurement as a function of momentum, angle, and cross section.

The relative momentum in the Λ-n system was computed for each event and enhancement factor in equation. 2.1.2 and was applied as a weight to the cross-section as each event was filled in the histograms.

2.1.3 Missing Mass

The top-left histogram in Figure 2.1 shows K^+ yield as a function of gamma beam energy (E_γ). The enhancement factors are greater in lower (E_γ) region (near the threshold), but still remain higher region. The lower histograms in Figure 2.1, are Λ-n missing mass distributions for two different (E_γ) ranges. It is clear that the yield was increased as a result of the FSI effect in wide region. The curves also indicate a need for 3 % accuracy in order to separate models, which is about 50000 events for every 100 MeV bin in (E_γ) .

2.1.4 K^+ Momentum

Theoretical studies show that the cross-section of K^+ differ in γ+d from γ+p as a result of the final state interaction (FSI), particularly, (1) in the production threshold region, and (2) roughly 10 times larger in forward and backward region in CM system.

Figure 2.2 shows scatter plots of the yield as a function of K^+ angle and momentum in the Lab. frame. The figures in top row requires a two-track trigger without Λ-n relative momentum cut. The (E_γ) ranges are shown in Figure 2.2. for each coloumn. The enhancement by the Λ-n FSI effect is evident in low Λ-n relative momentum region. The second to forth rows in Figure 2.2 correspond to different momentum ranges. The

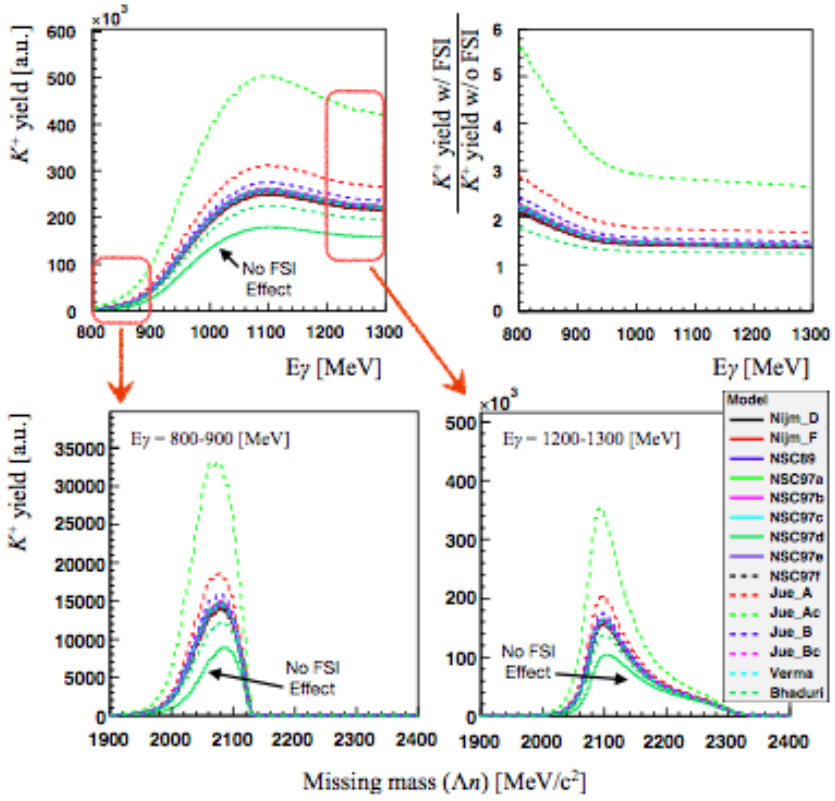

Figure 2.1: The K^+ yield as a function of gamma energy (E_γ) with various combination of scattering lengths and effective ranges (top-left). The enhancement factor as function (E_γ) (top-right). The bottom figures are the K^+ yield as a function of missing mass of Λ-n calculated from K^+ momentum. [5]

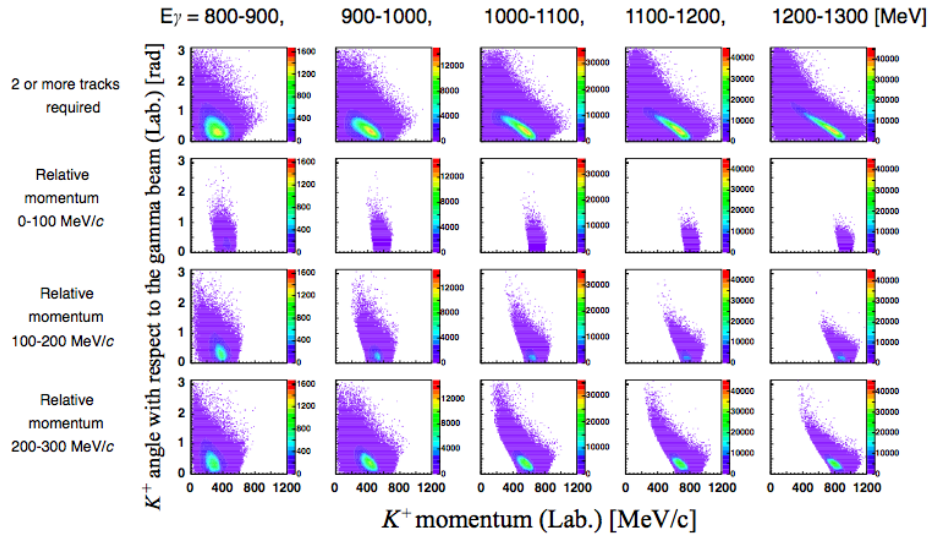

Figure 2.2: K^+ yield as a function of angle (0 to π rad) and momentum (0 to 1.2 GeV/c in the lab. frame.[5]

low relative momentum region is located in the forward angle region of K^+, but not restricted tot zero degree. It suggests that a wide coverage of acceptance is necessary to measure the FSI enhancement effect which is can be possibly measured by the NKS2 set up.

3

The Recent Apparatus of NKS2

3.1 Overview

This chapter deals with a detailed review of the recent experimental facility of the Neutral Kaon Spectrometer 2 (NKS2). The NKS2 collaboration has been studying the strangeness photoproduction in $\gamma + d$ reaction near the threshold [1, 2] at Research Center for ELectron PHoton (ELPH) Tohoku from 2004. The goal of this experiment is to understand the photoproduction mechanism of neutral kaon and the Λ hyperon in deuteron. NKS2 is a suitable spectrometer to measure the differential cross sections of the $\gamma(n, K^0)\Lambda$ channels. It will first give a brief overview of experimental techniques. This will be followed by an explanation of the tagging system and the generated photon beams, radiator and its control system, and the photon beam duty cycle. This will lead to a discussion about NKS2 spectrometer and its components. Furthermore, it would explain the improvement of some parts apparatus of the NKS2 spectrometer.

3.2 BST Tagger III and Photon Beam Line

The NKS2 spectrometer is located downstream of a real photon beam line in the second experimental hall at the Research Center for Electron Photon Science (ELPH) Tohoku University. The electron beam is accelerated up to maximum energy 1.3 GeV by LINAC (linear accelerator) at the first and then injected to the synchontron BST. Figure 3.1 shows the schematic view of the second experimental hall at ELPH.

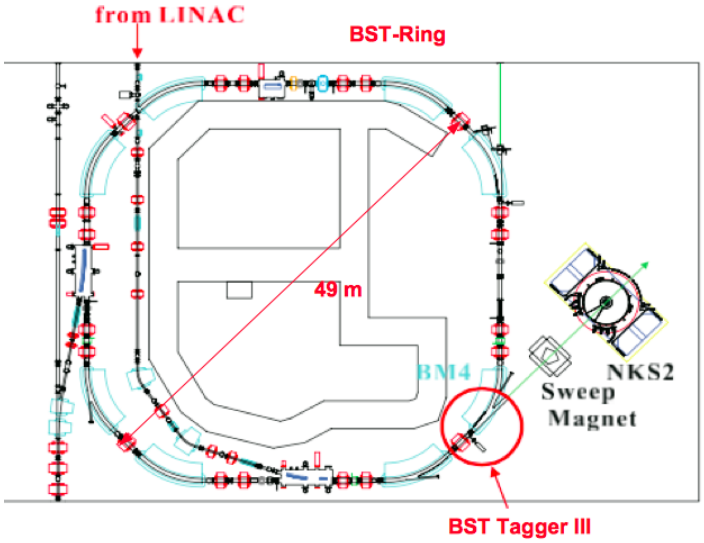

Figure 3.1: Schematic of the BST-ring, tagger system, sweep magnet, and the Neutral Kaon Spectrometer (NKS2) in the second experimental hall at the Research Center for Electron Photon Science

Radiator Control

The radiator is made of thin carbon wire. The insertion of the 11 μm carbon wire is controlled remotely by a computer in the counting room. During the electron injection and acceleration time the radiator is kept outside the electron beam path. A five phase stepping motor to which an aluminum frame is attached serves as transport for the carbon wire. The radiator movement has a maximum displacement of 100 mm and can be shifted in position at the highest velocity of 80 mm/s. The lower limit of the displacement in position that may be achieved is 2 μm [12]. For production experimentation periods, the usage of a continuous quasi-monochromatic photon is achieved by tuning the insertion speed and position.

BST Tagger III

Bremmstrahlung photon beams are generated at a target called as the radiator inserted in the electron beam line of the electron booster and storage ring (BST-ring). The electron detector is placed in the space between the pole and yoke of the fourth bending magnet (BM4) and detects momentum analyzed electrons after the bremmstrahlung and thus define timing and energy of radiated photons. The electron detector consists

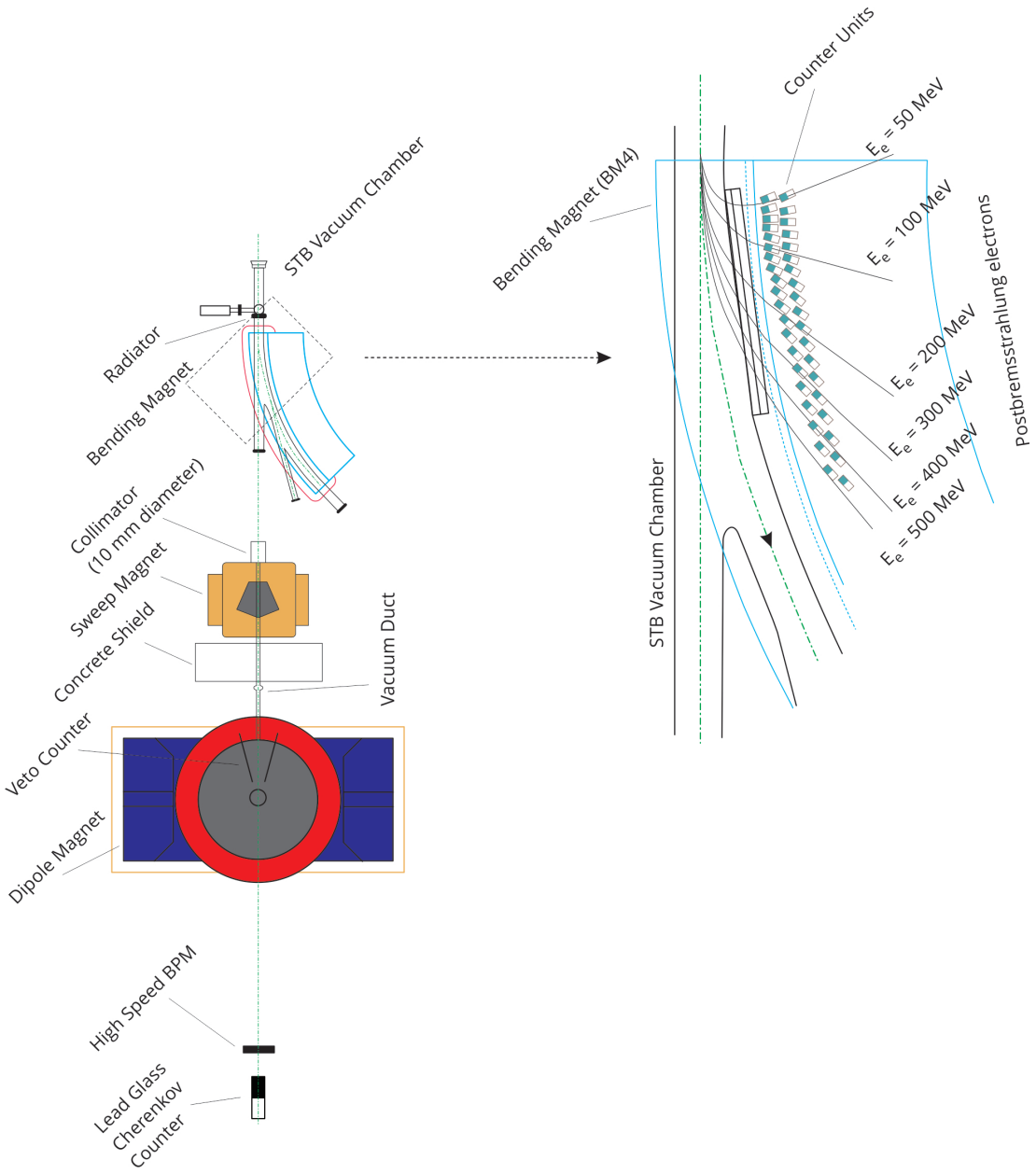

Figure 3.2: Schematic of the photon tagger package. A scattered electron will strike the scintillation counters, TagF and TagB, where its energy is determined by which segments it strikes, directly related to its deflection angle

of scintillation counters based on the Multi-Pixel Photon Counters (MPPCs). The read-out system for the timing counters (TagBs) consists of the ordinary leading edge discriminators. A differential amplifier circuit to reduce the pile-up of the MPPC signal with long tail and the dark counts of the parallel-connected MPPC array. The other read-out system for the position counter (TagFs) is EASIROC (Extended Analogue Si-pm Integrated ReadOut Chip) based electronics aiming at an easy operation easy operation of multi-channel counters. We designed an electron detector of the photon tagger composed of counter units each of which has one TagB and four TagFs. By a coincidence of a TagB and one of four TagFs belonging to one counter unit, a trajectory of an electron can be selected to reduce an electromagnetic background from electrons, positrons or gamma rays coming from other sources. Figure 3.2 shows a schematic view of the tagger.

Trajectories of electrons with energies after the bremmstrahlung emission of 1.31 GeV electrons on the radiator was calculated and the injection angles, positions and energy deposits of the electrons on the scintillators of the counter units were simulated. The maximum deviation of the injection angle was radians and the range of the photon beam was 0.78 to 1.27 GeV for electrons 1.31 GeV.

The electron was designed to have the following three functions:

- to align and fix the counter units on it,
- to hold connector changing circuit board, cables for signals, bias power, and preamplifier power,
- to align the base itself to the magnet.

Its shape had to fulfill the following requirements:

- compactness for the insertion through the limited space between the BM4 and a quadrapole magnet just (QC3) upstream of the BM4,
- sufficient length to fix all the counter units with the length of 1 m,
- avoidance of the matters which affect the magnetic field of the BM4.

Beam Position Monitor (BPM)

The Beam position monitor is composed of 16 finger counters that provide a two dimensional image of the photon incident position upon the target. It also incorporates a pair of trigger counters and a veto counter. During the experimental period, the BPM is monitored continuously to ensure the beam incident on the target is optimal.

Duty Factor

A typical beam cycle is presented in Figure 3.3 where the x and y- axis are the time and the beam current [I], respectively. The flat top and waiting time can be changed upon user request and is specified by a contacted power limit previously established with the electric power company of Tohoku area. The time for ramping both up and down area established ad 1.4 seconds. The flat top is typically 20 secs and waiting time is 8-20 seconds (these values are dependent upon the power supplied to the ELPH facility). The specific time that the radiator is placed in the path of the electron beam in calculated as the flat top -2 seconds.

Sweep Magnet

The large number e^-e^+ pairs that are created upstream from the photon beam is substantially reduced by placing the sweep magnet between the radiator and the spectrometer. It consists of a pentagonal shaped dipole magnet that generated a 1.1 Tesla field at 300 A in design. A scematic view and examples of deflection paths for several electron momenta are shown in Figure 3.4 . In front of the sweep magnet is a lead collimator comprised of 5 blocks, that reduce the beam halo. The collimator aperture is 1.0 cm in diameter. The sweep magnet being located before the main spectrometer efficiently suppresses the background contribution in the data and improves the data acquisition rate.

3.3 The NKS2 Spectrometer

The NKS2 was installed at the ELPH of Tohoku University. The NKS2 spectrometer consists of a dipole magnet, target cell for liquid deuterium, drift chambers, hodoscopes, and electron veto counters. Figure 3.5 presents a schematic view of the spectrometer.

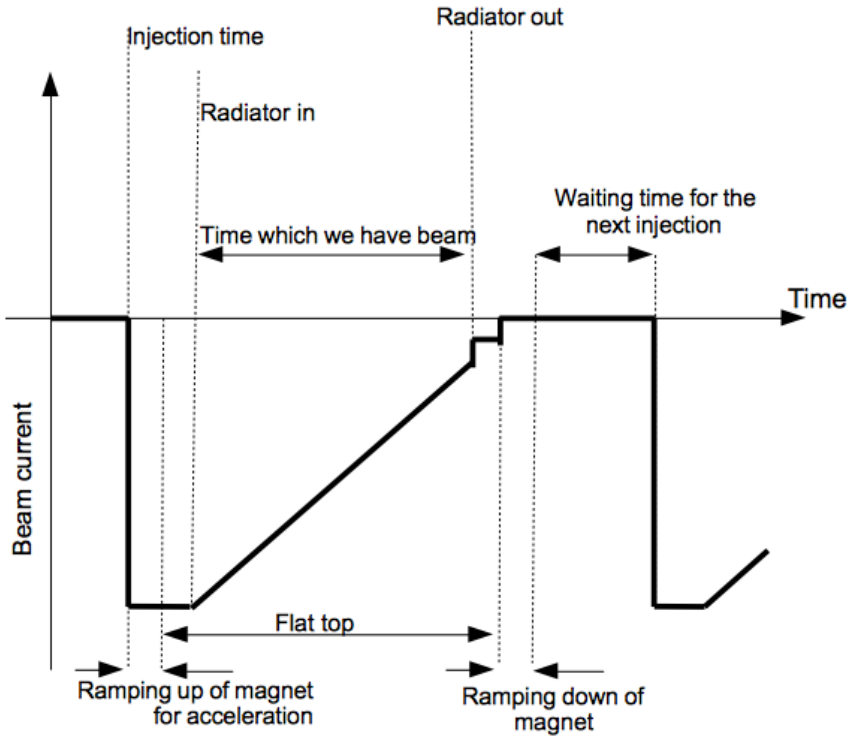

Figure 3.3: A time chart of the usual beam cycle.

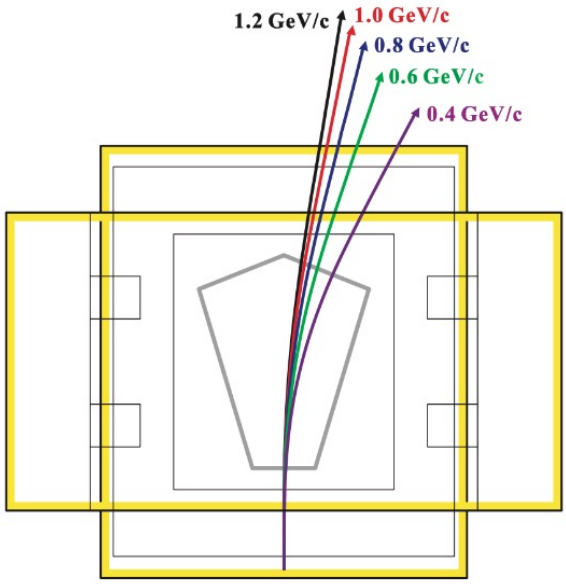

Figure 3.4: The sweep magnet and examples of deflection paths for various electron momenta

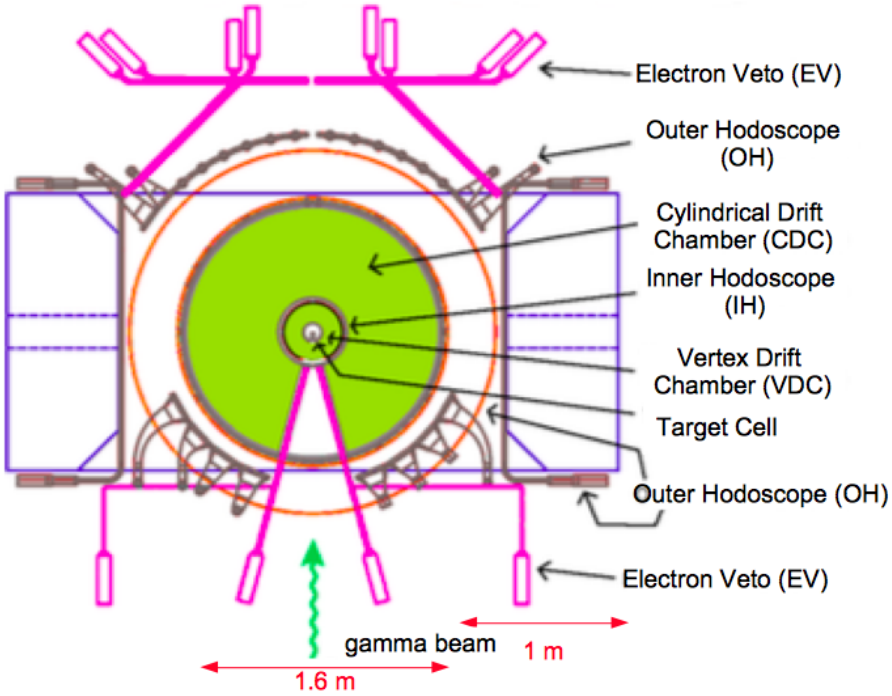

Figure 3.5: The schematic view of NKS2

The dipole magnet has a 680 mm gap and 800 mm diameter with a the magnetic field was 0.42 T at the center. The target cell is installed from topside of magnet yoke with the cryostat also being positioned on the top of the yoke. The NKS2 consists of 2 drift chambers, VDC and CDC, for tracking in the magnetic field. The IH and OH provides Time of Flight (TOF) information for a track associated with hits. The typical TOF resolution was on the order of 400 ps, which was sufficient to separate pions and protons in a momentum range less than 800 MeV/c. The EV counters were located on the beam plane and covered about 3 cm from the beam plane. They were introduced to reduce e^-e^+ background at the trigger level.

3.3.1 680 Dipole magnet

The NKS2 is designed around a dipole magnetic magnet. A downstream view of the 680 magnet is shown in Figure 3.6, where the magnet prior to the installation of the detectors is shown on the left and following the full installation of the detector package on the right. It generates a magnetic field of approximately 0.42 Tesla with a operational

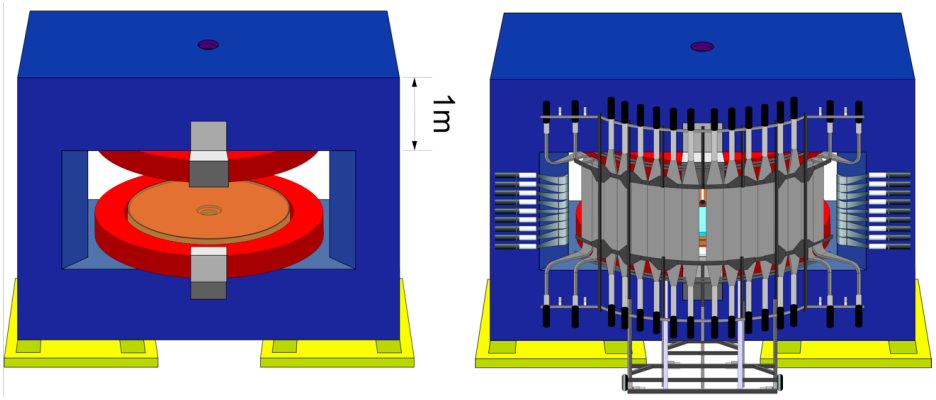

Figure 3.6: Dipole magnet is shown in the left figure prior to the installation of the inner detectors. The figure on the right illustrates the detectors installed with the OHV counters placed in their downstream location.

current of 1000 A. The magnetic field has been calculated by the TOSCA program. The dipole magnet has a vertical hole of 120 mm in diameter, located at its center, for the purpose of target insertion and removal.

3.3.2 Drift Chambers

The detection of particle tracks and their momenta are determined by the combination of a pair of drift chambers, the Cylindrical Drift Chamber (CDC) and the Vertex Drift Chamber (VDC). The fundamental principle lies in the ability of a drift chamber to detect a charged particle as it transits the detector by the ionization of the drift gas that produced a seed electron. This ionized electron is then multiplied resulting in an avalanche of electrons that are accelerator along the electromagnetic field lines and finally arrive at the anode wire of the chamber.

Drift Gas

The choice of drift gas was Ar+Ethane (50:50) which is also the same gas choice used in CDC. Full details of he drift gas properties can be found in reference [citation]. A cosmic-ray test of the VDC performance yielded a layer efficiency $\geq 99\%$ for all layers. We explored the option of changing the gas combination by introducing ethanol into the mixture.

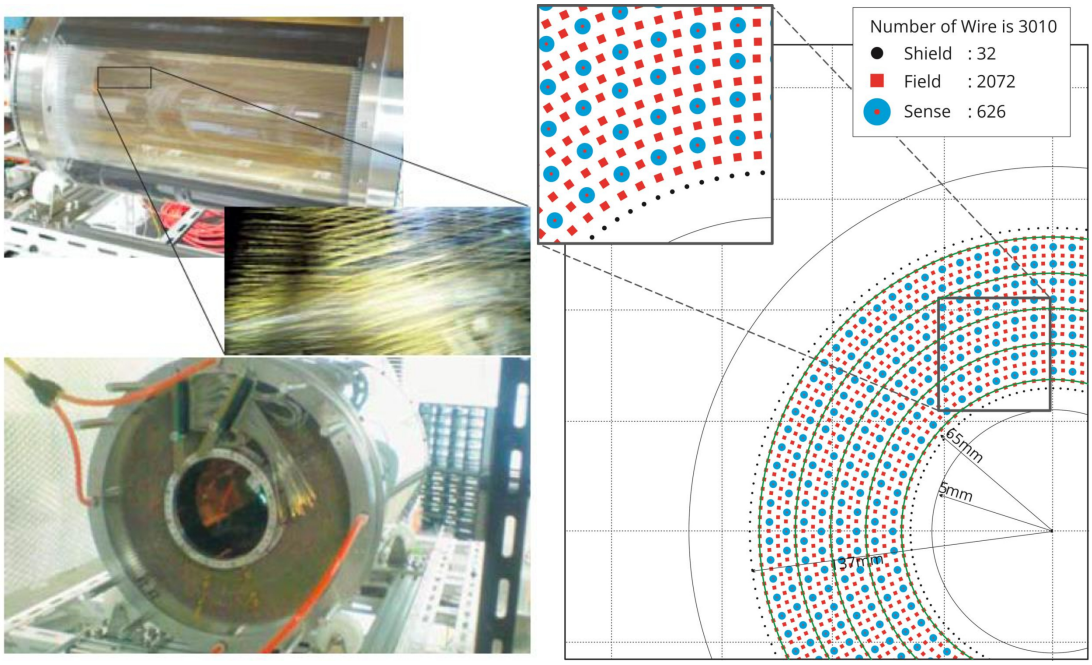

Figure 3.7: VDC detector and cell geometry shown left to right respectively.

Vertex Drift Chamber (VDC)

The spectrometer received an overhaul in the inner deyector sections the most important of which was installation of a drift chamber for vertex reconstruction and three dimensional tracking of the decay particles. Figure 3.7 shows the schematic view of VDC. The earlier drift chamber was a Straw Type Drift Chamber (SDC), that was capable of only accomplishing two-dimensional tracking.It is positioned inside Cylindrical Drift Chamber (CDC) and due to its unique design, will be capable of performing three-dimensional tracking of the decay particles.

Wire Geometry

The diameter of the VDC is 330 mm with a height of 506 mm and a solid angle about three times that of CDC. The detector is composed 626 sense wire placed at stereo angles such that they created eight layer. The cells are trapezoidal in shape with a half-cell size of approximately 4 mm. Each sense wire designed to have symmeteric wire alignment, hence threre were significant wire material on the beam line upstream of the target capable of contributing to photon conversion. In order to increase the

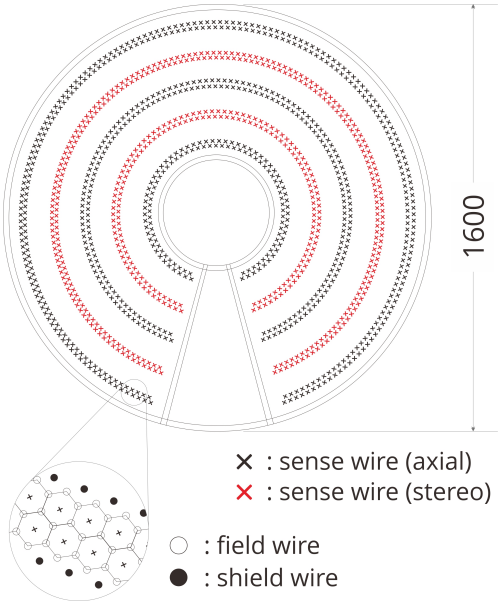

Figure 3.8: Schematic display of Cylindrical Drift Chamber (CDC), where the cell structure is shown on the lower left of the figure.

data acquisition capabilities the wires in the upstream direction along the beam line have been removed.

Read Out Card

A GNA-220 signal read-out card was designed to fit into the limited a space in the inner detector region. The GNA-220 has 32 channel inputs/digital outputs and used an Amplifier-Shaper-Discriminator (ASD) chip (SONY CXA3183Q) [13].

Cylindrical Drift Chamber (CDC)

The cylindrical honeycomb drift chamber (CDC), seen in Figure 3.8, is designed with a total diameter of 160 cm and consited of ten layers. These ten layers were furthered defined into a groups consisting of two layers within each group. The third of the group was titled at a stereo angle of 6.5 degrees. The angular of coverage of the chamber ranged from -165 - 165° in the horizontal direction, and radial coverage of 23.8-76.0 cm, from the edge of the field wire. Each sense wire was made from gold plated tungsten with a diameter of 20 microns with a set tension of 50 gw. Conversely, each of the shield and field wires were 100μm in diameter and made from Cu-Be (gold

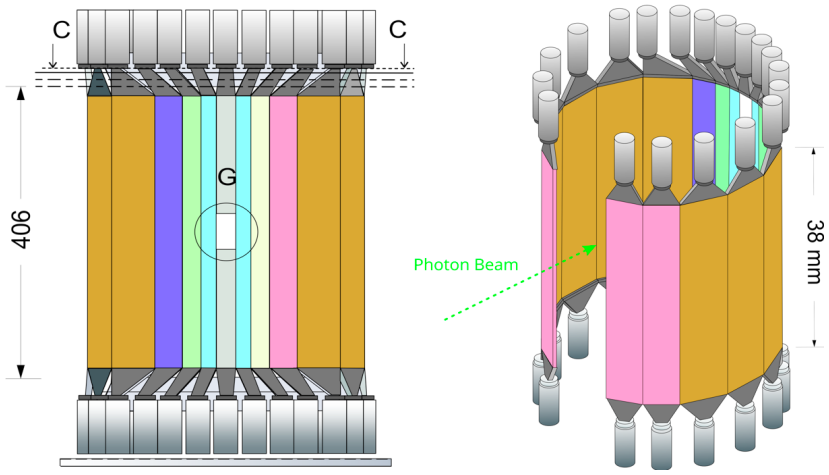

Figure 3.9: Full Inner Hodoscope (IH) assembled on the VDC

plated copper and berylium) with a set tension of 50 gw. The gas used was the same as for the VDC, and equally premixed combination of Argon and Ethane. The maximum drift time in a cell was roughly 250 ns. The combination of the CDC and VDC permits the tracking of charged particles in three dimensions, and are a necessary detector to measure the momentum and determine the decay tracks of the protons and charged pions.

3.3.3 Hodoscopes

In most spectrometers the position of particles are measured by hodoscopes, which are simply an arrangement of detectors to measure the position of a particle that is moving perpendicular its configuration.

Inner Hodoscope

The Inner Hodoscope, a Time Of Flight (TOF) counter, added into the logic as a start trigger. Each segment is attached to a light guide and a fine mesh dynode type photomultiplier, that operates on a negative high voltage setting and allows for operation within the 0.42 T magnetic field supplied by the 680A magnet. The IH counter segments are arranged to enclose the VDC. The size of each segement was specifically designed considering the probability of multiple hits on one segment and the PMT peak operational singles rate. The desired requirement was that of a less than 2% probability

of multi-hits and a singles rate $\leq$ 200 kHz. The reduction of multiple hits n one counter is necessary to avoid discarding $\pi^+ pi^- \pi^-$ events, where two or more decay particles transverse the same IH segment. IH (5-8) have scintillators $38.0^H \times 7.53^W \times 0.5^T$ cm in size. IH2 is $32.0^H \times 1.83^W \times 0.5^T$, and was designed with a thinner width, 1.83 cm, than the remaining segments to reduce the counting rate. The result of a GEANT4 simulation revealed that the incoming bremmstrahlung photons of energy of 5MeV to 1.2GeV resulted in a singles rate of 160 kHz at a tagged photon rate of roughly 2 MHz. Figure 3.9, presents the all IH counters mounted upon VDC body.

3.3.4 Outer Hodoscope

As the IH used as a start counter, the outer hodoscope (OH) is used as stop counter and is a necessary part of the trigger system in that it was able to detect two particle existing the inner detector package sufficiently providing coverage of $\pi^+\pi^-$, $p\pi^-$ or four particle decay event. The OH is constructed from two sections one of which is arranged in a vertical position (OHV) and the other arranged horizontally (OHH) and further divided into right and left components. The vertical component consisted of a total of 24 segments, having 12 arranged on either side of the beam line, defined as outer hodoscope vertical left (OHVL) and right (OHVR). OHV 1-8, use scintillator counters of $74.8^H \times 7.53^W \times 2.0^T$ cm in size, and are placed downstream in relation to the target position. OHV 9-12 are placed upstream and have scintillators $50.0^H \times 5.64^W \times 2.0^T$ cm in size. The orientation of OH counters is shown in Figure 3.10 . The horizontal component oh the OH had 9 segments for the left and right side, and since they were arranged parallel to the beam direction, they would detect particles with a high curvature. The OHH counters that were arranged on the plane of the beam line were thinner in design for the purpose of lowering the count rate. OHV 7-12 and all OHH plastic segments were affixed to folded light guides in order to transport the signals outside of the magnetic dipole region because of a photomultipliers performance sensitivity to strong magnetic fields. The vertical segments were 60 cm in height and 2 cm in thickness.

3.3.5 Electron Veto (EV)

The photon beam will contribute a lot of background signals via the pair production process and was be the main contamination at the trigger level. In an attempt to

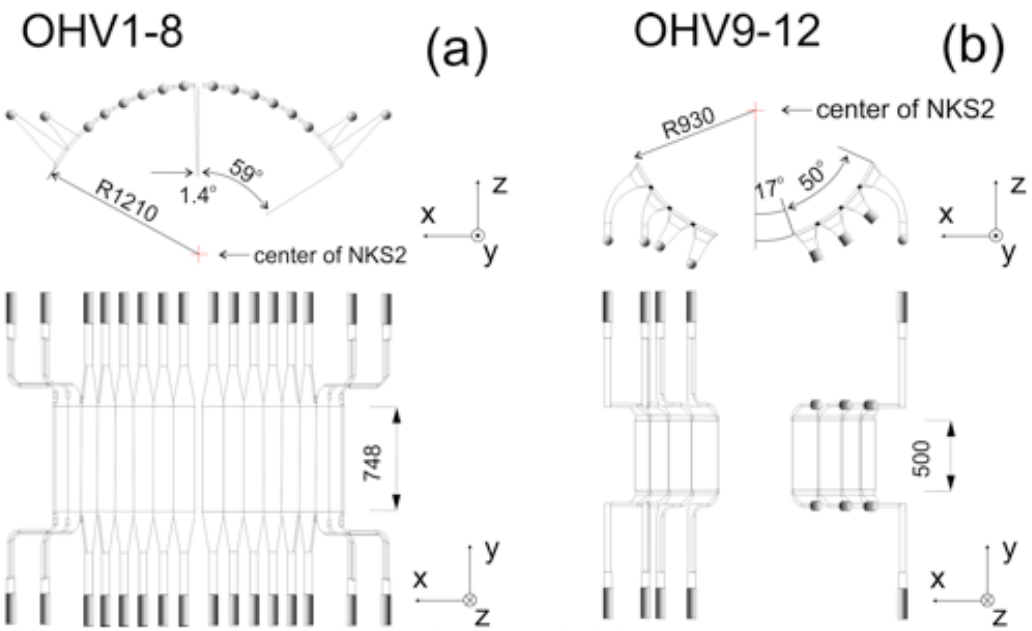

(a) Outer Hodoscope Vertical Components

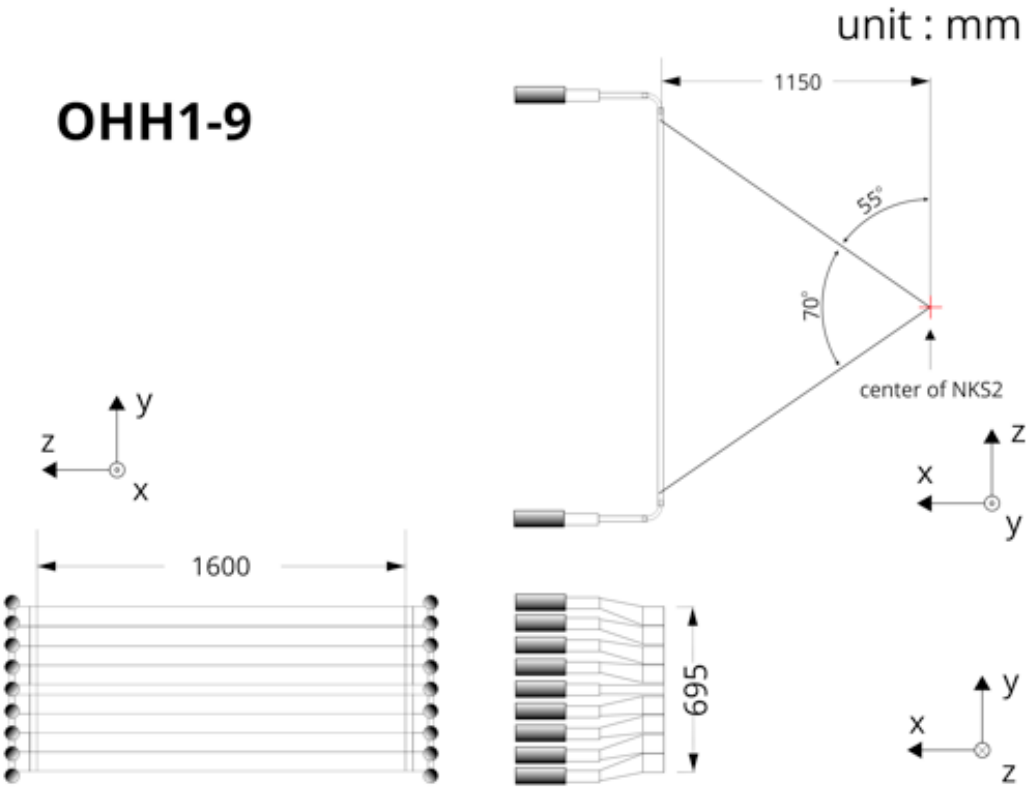

(b) Outer Hodoscope Horizontal Components

Figure 3.10: Outer Hodoscope (OH) detector package orientation

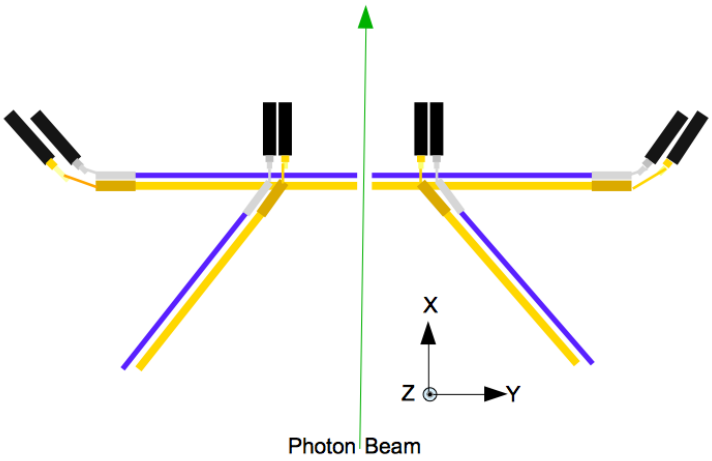

Figure 3.11: Electron veto counters 1 and 2

reduce this, an electron veto counter was constructed. The light mass of the electrons will result in a small opening angle for the created pairs. The EV was placed on a zero degree plane perpendicular to the beam line. There are 8 detectors arranged in four pairs that comprise the entire EV package, referred to as EV1 - EV4, where the numbering of the counters grows in relation from the downstream to upstream potion. Detailed of the EV counters illustrated in Figure 3.11. The aim is to reject electron and positron pairs because the conversion probability is much larger than the $\gamma n \rightarrow K^0\ \Lambda$ reaction. However, there is the chance of discarding pions and proton from K^0 and Λ. The Λ hyperon is produced primarily in the forward direction. It follows then that the proton from the Λ particle will move forward especially in comparison to the charged pion decay from the kaon. Consequently, the use of the EV counters downstream has been eliminated and a study was performed to ascertain the effects of their removal from the trigger in terms of the data acquisition capabilities.

3.3.6 Target System

In order to study the photoproduction reaction process on a neutron, it was decided to use the deuteron, the simplest bound system of nucleons. The cross section of K^0 Λ is roughly on the order of 1 μb . Therefore, in order to obtain a significant amount of statistics, not only is it necessary to have a beam of the highest intensity possible, but a dense target should also be used. The target system was used to condense the

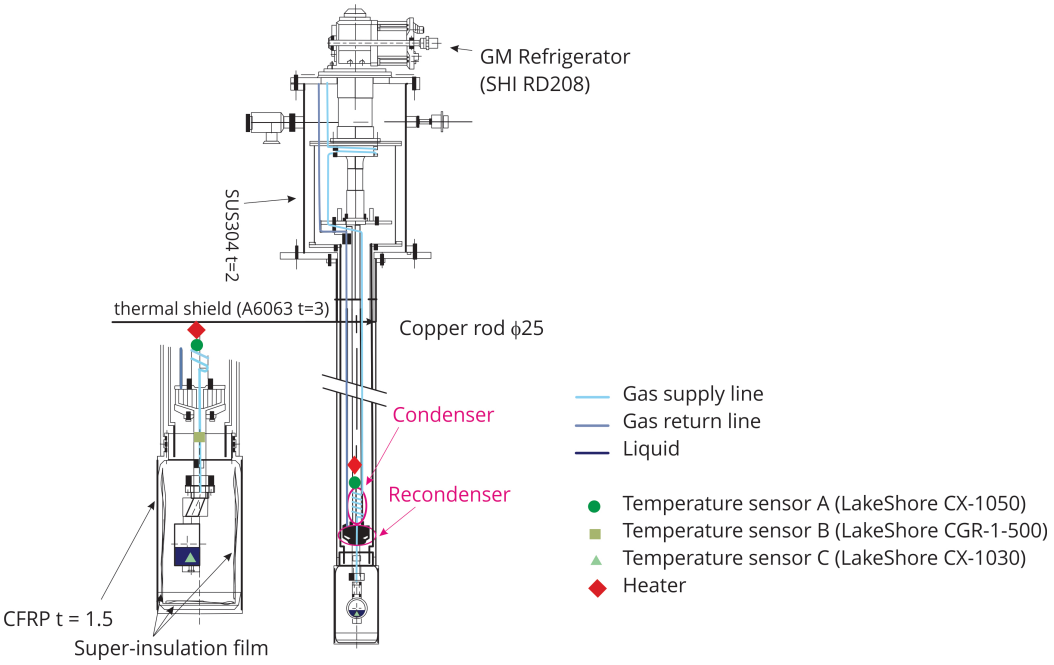

Figure 3.12: The target is stored in the vacum chamber below the recondenser and was designed to be inserted and removed from the spectrometer via an aperture located at the top by a manually operated crane system.

deuterium into liquid form. The target is housed in the vacuum chamber placed under the recondenser. The apparatus was designed to be inserted and removed from the spectrometer via an aperture located at the top by a manually operated crane system. The target system and the inner details are shown in Figure 3.12.

The target cell is monitored remotely by National Instruments LabVIEW on a Linux machine in the counting room due to the inaccessibility of the experimental hall during the target irradiation period. Constant monitoring ensures that the target is maintained at a safe operational temperature and does not solidify. During the course of the experimental runs the target temperature and absolute pressure were monitored enabling the calculation of the density of the liquid deuterium target and subsequently the number of the target neutrons. The vacuum chamber, cylindrical in shape, was designed with a thickness of 1.5 mm. It was inserted through a vertical hole in the spectrometer with a diameter of 120 mm, located 15 mm from the center position of the NKS2 into the magnetic yoke, in a configuration such that its axis was parallel to that of the beam line, for the purpose of increasing the photoinduced production of

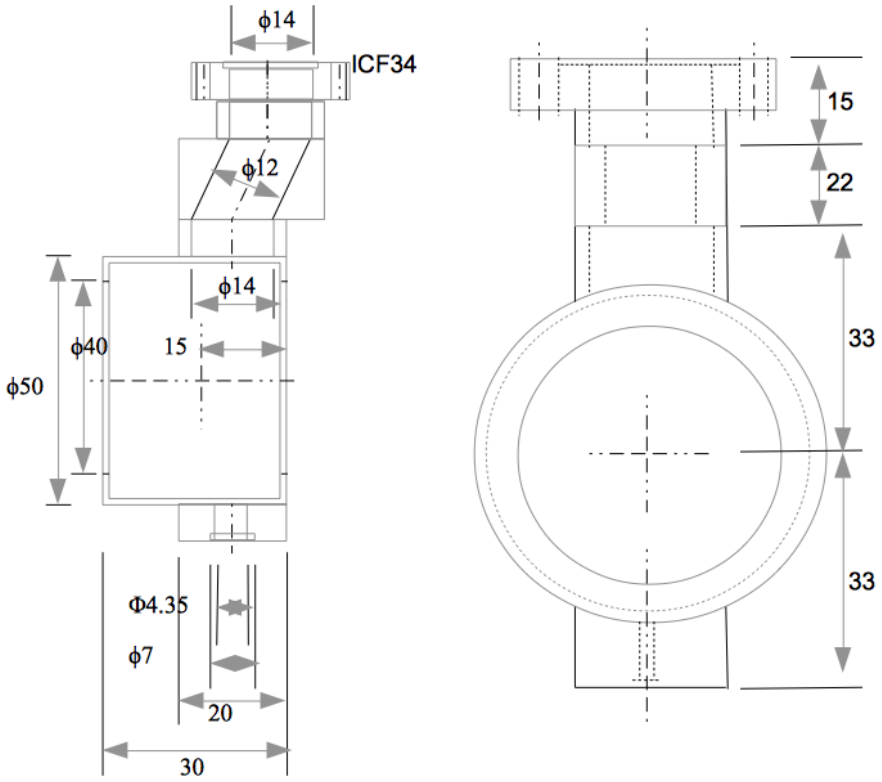

Figure 3.13: Shape of target cell.

K. The deuterium in a gaseous state is injected by an inlet port and liquified at the condensor and allowed to drip into the target cell]. The target cell is constructed from aluminum with an outer shell thickness of 1 mm and a beam window constructed of Upilex-S film 75m in thickness clearly visible in Figure 3.13. The beam window was designed to 40 mm and the outer diameter of the cell is 50 mm. The target thickness is designed to be 2.97 cm.

3.4 Triggered Event and Associated Electronics

Electronics and Data Acquisition (DAQ)

A trigger is usually a set of detectors that works in combination to indicate when an event of significance has taken place. The trigger determines when the signals of the detector package should be recorded, where the aim to gather the largest yet cleanest data set at the highest beam intensity possible. Therefore, an ideal trigger would

eliminate the recording of events not of interest, and increase the retrieval of events that may contain information regarding the physics to be explored. The UNIDAQ on Linux was used as a base system of the NKS2 data acquisition system. In the experimental counting room the data is collected on three data acquisition machines, which are designated as k0daq0, k0daq1, and k0daq2. Both k0daq0 and k0daq1 are used to record data from the drift chambers and k0daq2 is used for the IH, OH, and EV signals and scaler data.

Trigger

The trigger logic differed for various data that desired to be taken. As such, full diagrams of the upgraded NKS2 logic for production data, tagger system calibration as well as for the counters and chambers. The main trigger utilized for physics production experiments required an event trigger from the STB tagging arm and the spectrometer arm. The tagging system portion required an event trigger that was made from a coincidence between the TagF and TagB counters in order to decrease the background and in principle, a tagged electron will have approach on a deflection angle the a photon was produced in the 0.8 - 1.1 GeV energy range. The trigger requirement on the spectrometer half prescribed that even with to or more charged particles were detected that transferred the spectrometer. Therefore two more particles were required from the IH and the OH counters. It is possible to also include the signal from the EV counters as a veto of electron coming from photon conversion. We implemented a spill gate, connected with the beginning motion of the radiator to repudiate events that originated from the radiator itself. The EV is included into the trigger logic as a veto. Thus, if there is a recorded coincidence event by the left and right EV counters the trigger is not provided.

Tohoku Universal Logic Module (TUL)

A programmable logic unit, referred to as the Tohoku Universal Logic module (TUL-8040) was used in the various trigger logics of the NKS2 spectrometer. The module has the capabilities of several module that are each accessible by switching amongst the installed programs. The propagation time within each module in approximately 50 ns. It was designed with 80 input (ECL/LVDS 64 ch + NIM 16 ch) and 40 (ECL 32

ch + NIM 8 ch) output channels, that are mounted to a FPGA (Field Programmable Gate Array) chip of a ALTERA APEX 20 series.

3.5 Time Resolution

The current status of NKS2, kaon identification is still very difficult on mass square spectrum because IH and OH time resolution are not enough to separate kaon, pion, and proton. So we want to enhance NKS2 Time of Flight (TOF) resolution to can separate kaon from other particles. The typical TOF resolution (σ) of IH and OH was on the order 400 ps, which was sufficient to separate pions and protons in a momentum range less than 800 MeV/c.

3.6 Improvement of Experimental Design

By using Multi-gap Resistive Plate Chamber (MRPC), we expect that can enhance the NKS2 TOF resolution less than 100 ps (so it is easy to identify kaon) and measure the $\Lambda - n$ interaction in $\gamma d \rightarrow K^{+}\Lambda n$. From design of an experiment to study the $\Lambda - n$ interaction via Final State Interaction (FSI) with the GEANT4 simulation, we can compare the result of the new design with the theoretical estimation, and also we can confirm that it is consistent with the theory.

4

Design of the New Experiment

4.1 Upgrade Plan

By using the recent NKS2 experimental setup, we can measure the effect of Final State Interaction (FSI). However, to measure the FSI effect more precisely, we want to produce and detect K^+ as many as possible. Photoproduction cross section is small so that time K^+ yields per 1 day with limited beam time.

We use particle identification (PID) to identify K^+. For measuring K^+, we need better resolution of Time-of-Flight (TOF) counter. Recently, we use Inner Hodoscope (IH) and Outer Hodoscope (OH) for TOF counters at NKS2, but these counters do not have enough time resolution to separate π, K, and p with mass square spectrum for PID as shown in Figure 4.1 [14]. K^+ is buried in the mass square spectrum. Indeed, by applying several very tight cut conditions, we can select K^+. But in adding cut condition process, we suffer loss from the view of the yield of K^+. However, if we can decide K^+ on mass square spectrum without tight cut conditions, the yield of K^+ may increase comparison with before. Mass square resolution is mainly decided by time resolution, momentum resolution, and position resolution. Momentum resolution and position resolution is decided by drift chambers because we measure momentum and path by tracking, and these resolution value is good as such. However, time resolution is worth and we can improve. So we want to make new counter, MRPC to improve time resolution. Figure 4.2 shows a prototype of the detector that has the following characteristics:

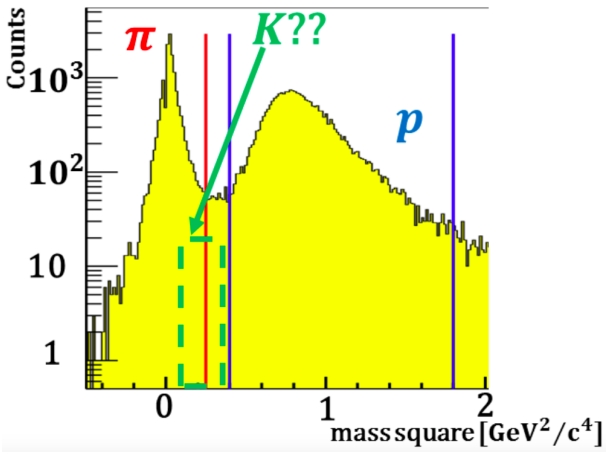

Figure 4.1: Current NKS2 mass square spectrum for π, K , p using IH ($\sigma_{ave} \approx 200$ ps) and OH ($\sigma_{ave} \approx 400$ ps)

- good time resolution to separate π, K , p in the mass square spectrum ($\sigma_{ave} \approx 100$ ps),
- cover large area,
- tolerance under magnetic field

MRPC is gas detector which use gas multiplication. When high energy particles, such as cosmic ray or particles populated photoproduction through MRPC, particles ionize gas molecule. Electron and ionized molecule (which has plus charge) are made by that process. Electron and charged molecule are accelerated by electric field made by anode and cathode. Electron goes to the direction of anode and charged molecule goes to the direction of cathode. When accelerated charged particles hits another gas molecule, gas another e^- and charged molecule are populated, so that process occurs many times. This is the principle of gas multiplication and many e^- (or charged molecules) will be populated. We detect many e^- as signal of MRPC.

Time resolution of MRPC will be decided by gap size, the number of gap, and read-out pad size. For read-out pad size, this is qualitatively discussion, but the smaller pad size MRPC can achieve the better time resolution. For gap size, we discuss about time resolution about each gap. Assumed that gap size is 250 μm, e^- drift velocity is 200 μm/ns, and e^- which can be detected as MRPC signal is populated round the place of 10 % cathode gathering. By these assumptions, uncertainty of initial populating

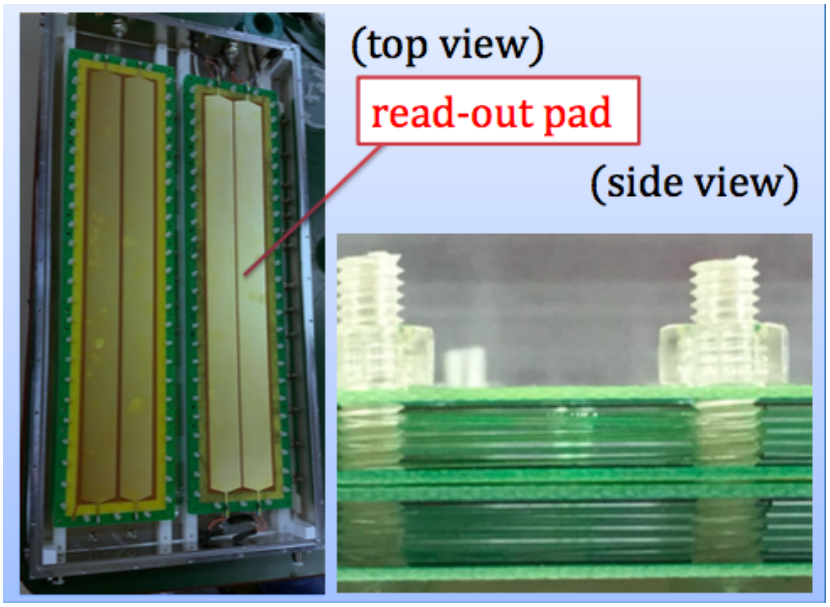

Figure 4.2: Picture of Multi-gap Resistive Plate Chamber

position of e^- which populated from ionization is 25 μm. So drift time of 25 μm correspond to 25 μm/200 μm/ns $\sim$ 130 ps. If distribution form of uncertainty of initial populating position of e^- is uniform distribution, standard deviation is calculated by $130/\sqrt{12} \sim 40$ ps, which is time resolution (σ). This point is time resolution of each gap depends on gap size and its value has good resolution. For the number of gaps, this can be explained by statistic. Ionization reaction by charged particles can occur at gaps, so the number of gaps corresponds to the number of e^- by ionization. Time resolution depends on statistic number of e^- (same meaning as large signal of MRPC), so the large number of gaps is better from the view of time resolution.

Structure of MRPC is as shown in the Figure 4.3:

- read-out pad: 45^H cm $\times$ 3.6^W cm (rectangular part) + base 3.6 cm, height 5 cm (isosceles triangle part)
- 5 gaps $\times$ 2 stacks
- HV = $\pm$6500 $\sim$ $\pm$8000 V
- gas between read-out pads = 2 mm
- gas: mixture of 90%Freon 134a CH_2FCF_3 and 10%SF_6

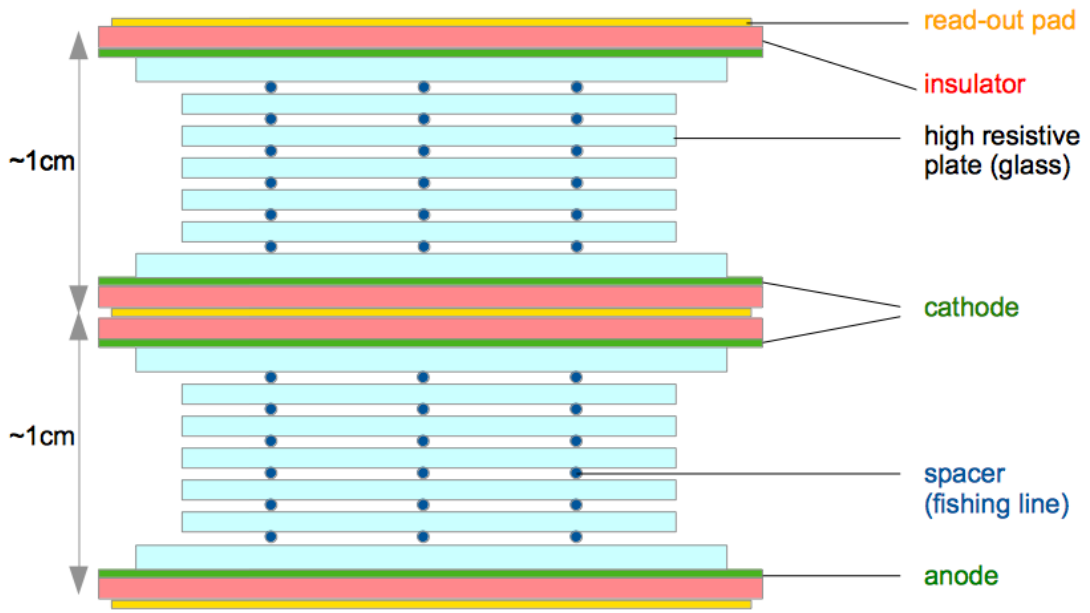

Figure 4.3: Schematic vew of Multi-gap Resistive Plate Chamber

- high resistive plate: glass (thickness = 0.4 mm)
- spacer: fishing line ($\phi \sim 235\mu m$)
- electrode: carbon type (thickness = 90 μm)

We have a plan to replace OH with MRPC to improve time resolution and select kaon more precisely without reducing a peak count by the cut conditions. The mass squared distributions was defined by the following equations 4.3.2, where fitted to a Gaussian function with assumption time resolution is 100 ps. Distributions for the mass square of the charged particles observed by the spectrometer is shown in Figure 4.4. From this simulation,we can separate kaon by good time resolution detector. So, we can ensure that MRPC can be applied to improvise NKS2.

4.2 Set Up in the GEANT4 Simulation

GEANT4 is a toolkit for simulating known physical processes using Monte Carlo (MC) method, and is the most widely used simulation tool in nuclear or particle physics field.

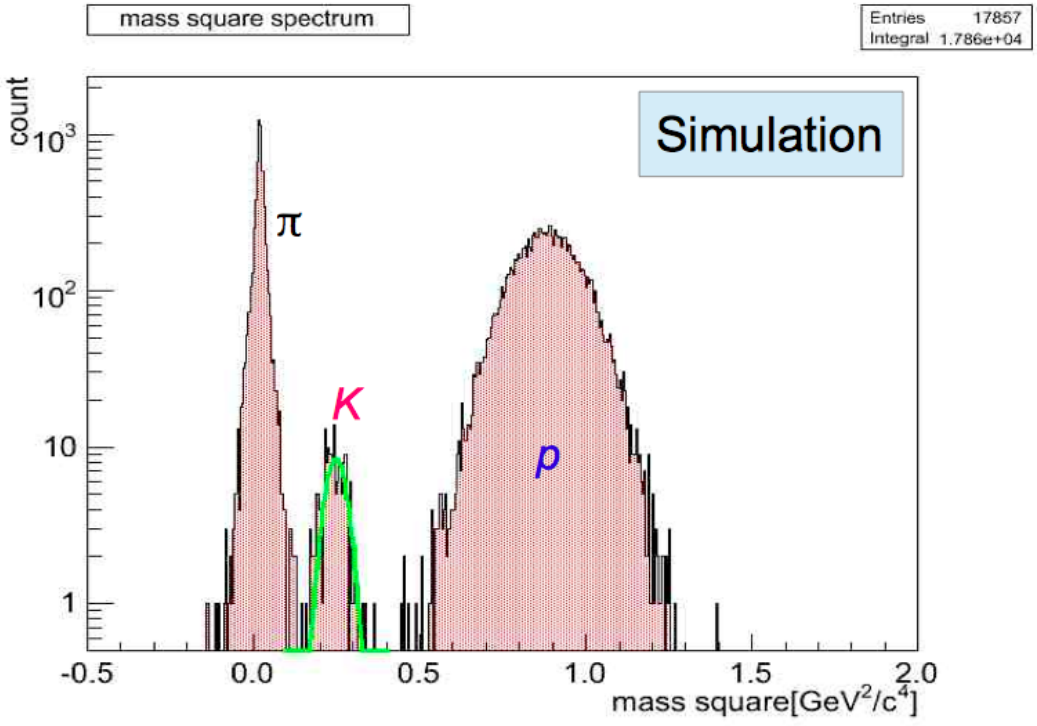

Figure 4.4: The result of simulation with σ=100 ps.

GEANT4 has several convenient applications for users, physics process information for example. By using GEANT4 simulation, we can simulate the reaction events in an intended/planed experimental or detector geometry. By using GEANT4 simulation, we can simulate the reaction processes, so we can study feasibility of FSI in the NKS2. By this simulation, we can see separation of kaon by using mass square plots with assumption time resolution, we will get the value of multi nhit probability can be accepted which correspondence between the number of segment and pad width, we will get the best acceptance by changing the radius of MRPC, and we will also know contamination ratio dependence of radius.

4.2.1 Detector Set Up

We studied an acceptance of new setup using MRPC. As the first step the we use a cylinder detector with number of segment (segnum) being 202, the angle coverage of the detector is 360 degree. We change the radius/distance from the center (target position) to MRPC in order to optimize the distance against background events. We set the height of MRPC by using (diameter/1200)x748 mm, where 1200 and 748 is default radius and height of previous detector (OH), respectively.

4.2.2 Probability of Multi hit

If we change the number of segment, the width of each segment of the cylindrical detector (MRPC in this simulation) change accordingly, which then is related to the probability of multi hit events. So, we can estimate the probability of multi hit by changing the segment number. The probability of multi hit is define by ratio of the number of events that multi hit occur between the number of events that more than 1 particle hit a MRPC. From Table 4.2.2, we know that probability of multi hit will be decrease if the segment number increase. It means that probability of particles hit in the same event will decrease if the number of segment of MRPC larger. We expect to get the small value of probability multi hit for separating the particles. So, from Table 4.2.2 we can know that by applying 12 number of segment, we will get big multi hit, is around 16.6 %. On the other hand applying 502 number of segment is so difficult for this setup. So, the reasonable number of segment are around 202.

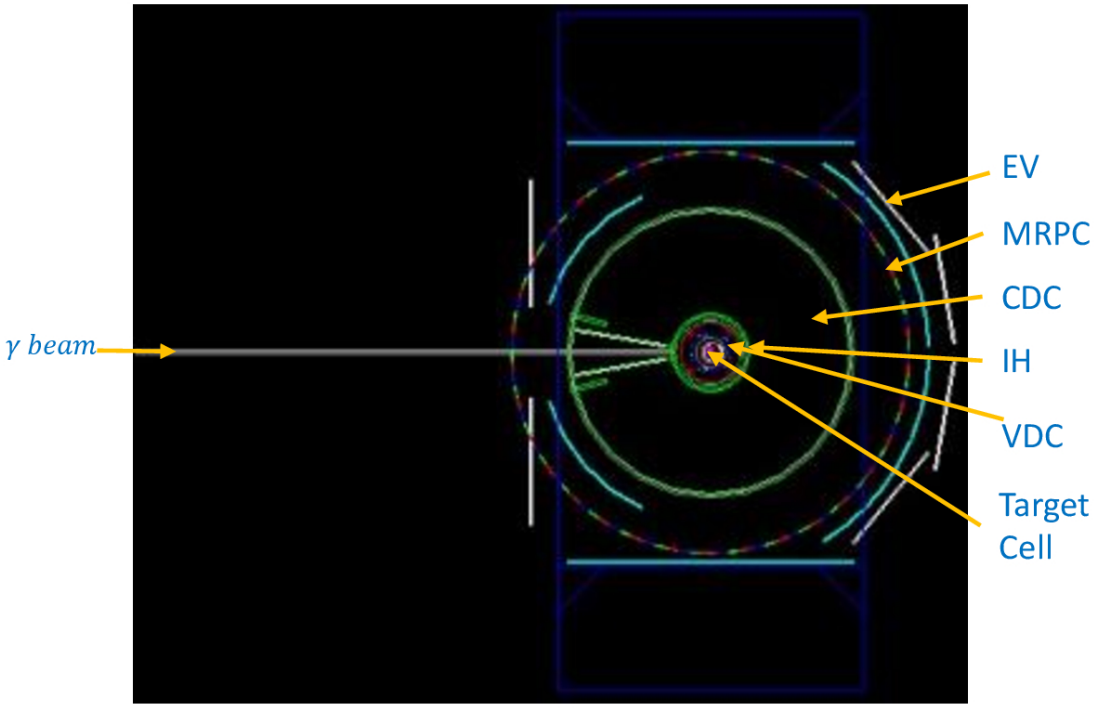

Figure 4.5: NKS2 Detector Construction: SetMRPC

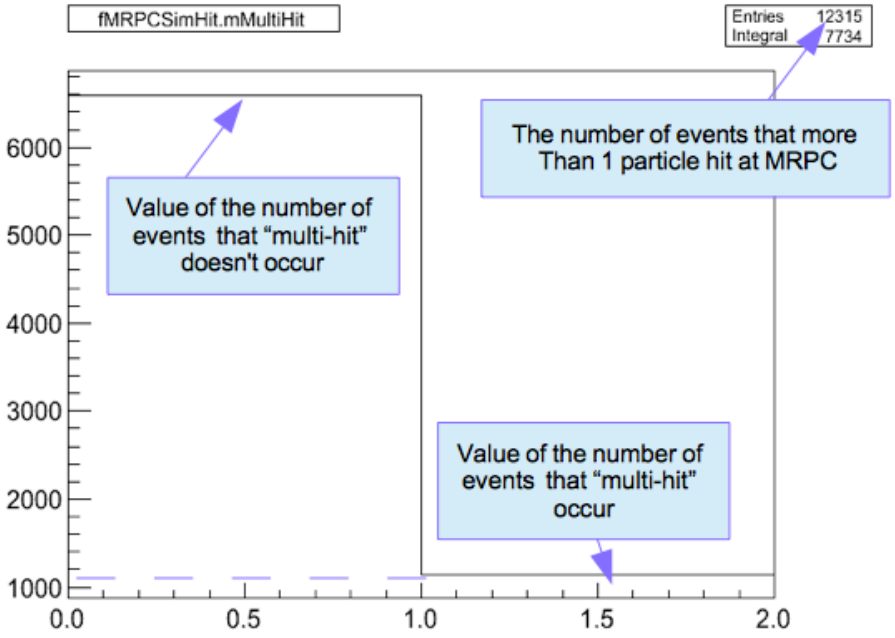

Figure 4.6: Histogram to get information about probability of multi hit

The number of segment	Multi hit	More than 1 particle hit at MRPC	Probability of multi hit (%)
12	1264	7520	16.8
52	348	7488	4.6
102	108	7496	2.6
202	133	7477	1.8
502	68	7540	0.9

4.2.3 Radius Parameter Changes (Geometry Construction Acceptance)

Acceptance refers to purely geometric fiducial volume of the detector. Solid angle is subtended by a cylinder of height H and radius R at the center of the cylinder. The cylindrical wall covers a spherical zone of height H from a sphere of radius $\rho = \sqrt{R^2 + \frac{H^2}{4}}$. The area of this zone is then $A = 2\pi H\rho$, and its spherical angle to:

$$\frac{A}{\rho^2} = \frac{2\pi H\rho}{\rho^2} = \frac{4\pi H}{\sqrt{4R^2 + H^2}} \tag{4.2.1}$$

- Radius: 1000 mm=1.40π sr
- Radius: 1100 mm=1.29π sr
- Radius: 1200 mm=1.19π sr
- Radius: 1300 mm=1.10π sr
- Radius: 1400 mm=1.03π sr

By geometrical calculation, acceptance will be larger if the radius of detector smaller keeping its height same. If radius of detector smaller (distance between target and MRPC), so the path length will be shorter too. Resolution become worth if path length (distance between IH and MRPC) is short. It means beta resolution become worth as the path length become shorter. On the other hand, we do not set the radius of MRPC to small size, because mass resolution depend on beta and beta resolution (Equation 4.3.1). So we should search best point satisfying better acceptance and resolution.

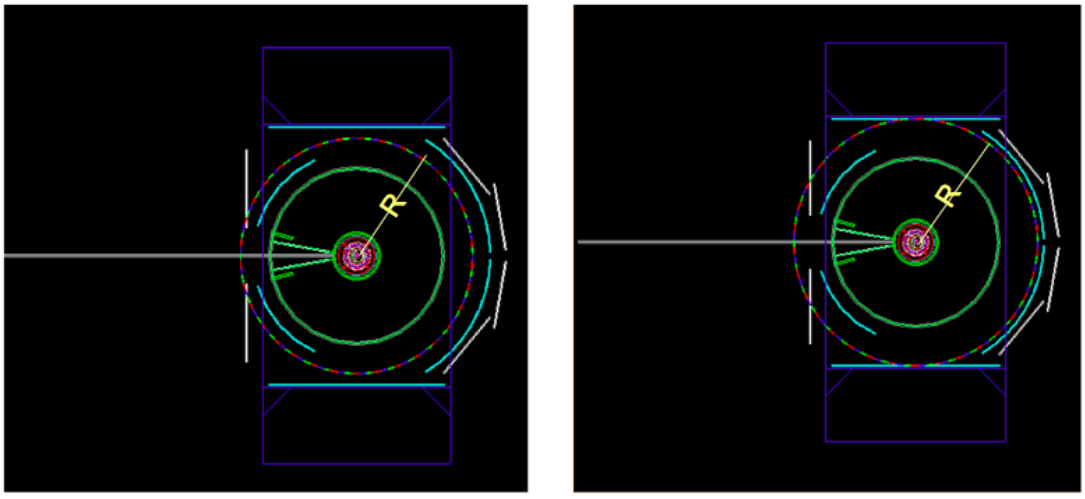

(a) Radius: 1050 mm (b) Radius: 1150 mm

Figure 4.7: Radius parameter of MRPC changes

4.3 Expected Result

4.3.1 Expected Particle Identification (PID)

TOF

Time-of-Flight measurement allows for a particles mass to be determined by knowledge of flight time, the momentum, and the path length, and thus can identify the particle species. From the energy-momentum relation the velocity can be calculated as,

$$\beta = \frac{p}{E} = \frac{p}{\sqrt{p^2 + m^2}} \tag{4.3.1}$$

Therefore, the square of the particles mass is found by.

$$m^2 = \left(\frac{p}{\gamma\beta}\right)^2 = p^2\left(\frac{1}{\beta^2} - 1\right) \tag{4.3.2}$$

Contamination Ratio Dependency on the Position

By changing distance from the center (target position) to MRPC, we roughly estimated that pion, Kaon, and proton are separable on these mass square spectrum as shown in Figure 4.8, where TOF resolution is fixed with σ=100 ps. From this mass square spectrum plots, we can see the value of contamination depend of position.

The contamination is defined as:

$$\text{contamination} = \frac{\text{the number of pion in kaon spectrum} \pm 3\sigma}{\text{the number of kaon in kaon spectrum} \pm 3\sigma} \tag{4.3.3}$$

We got relation between radius and contamination from Figure 4.9. The contamination will be decrease if the radius larger. It means that pion and kaon can separate well if the radius of detector is large. As we can see that 1.4 m will only have 1.1 % contamination. But, in NKS2 we have limit space for putting the cylinder detector inside the dipole magnet. So, the posibility to get minimum contamination is 1.2 m.

4.3.2 Kinematic Region of K^+

The effect of FSI is expected to be large in forward region [15]. To check how the effect can be seen in the NKS2 acceptance, we checked K^+ yield for different $\Lambda - n$ relative momentum region.
Figure 4.10 shows scatter plots of the yield as a function of K^+ scattering angle and momentum in the laboratory frame. In the figures at the top row, a two-track trigger without $\Lambda - n$ relative momentum cut is demaded. Equation 2.1.1 gives a large FSI enhancement in the small $\Lambda - n$ relative momentum region. Therefore, we select different regions of relative momentum. In the second row, a two-track trigger with relative momentum of 0-100 MeV/c, the 100-200 MeV/c for third row, the 200-300 MeV/c for the fourth row, and relative momentum more than 300 MeV/c were demanded for the fifth row. The E_γ ranges are shown in Figure 4.10 for each coloumn.

The enhancement by Λn FSI effect is evident in low Λn relative momentum regions. The second to the fifth row in Figure 4.10 corresponds to different momentum ranges. The small angle (respect to the gamma beam direction) region of K^+ in lab. frame is corresponding to small Λn relative momentum region. It is due to Lorentz boost. In the low relative momentum region, events are located in the forward angle region of K^+ but not only at zero degree. It suggests that a wide coverage of the acceptance is necessary to measure the FSI enhancement effect, which can be measured by the NKS2.

This is an advantage of NKS2. The other experiment, for example, JLab type spectrometer has higher momentum resolution and higher beam intensity, but those

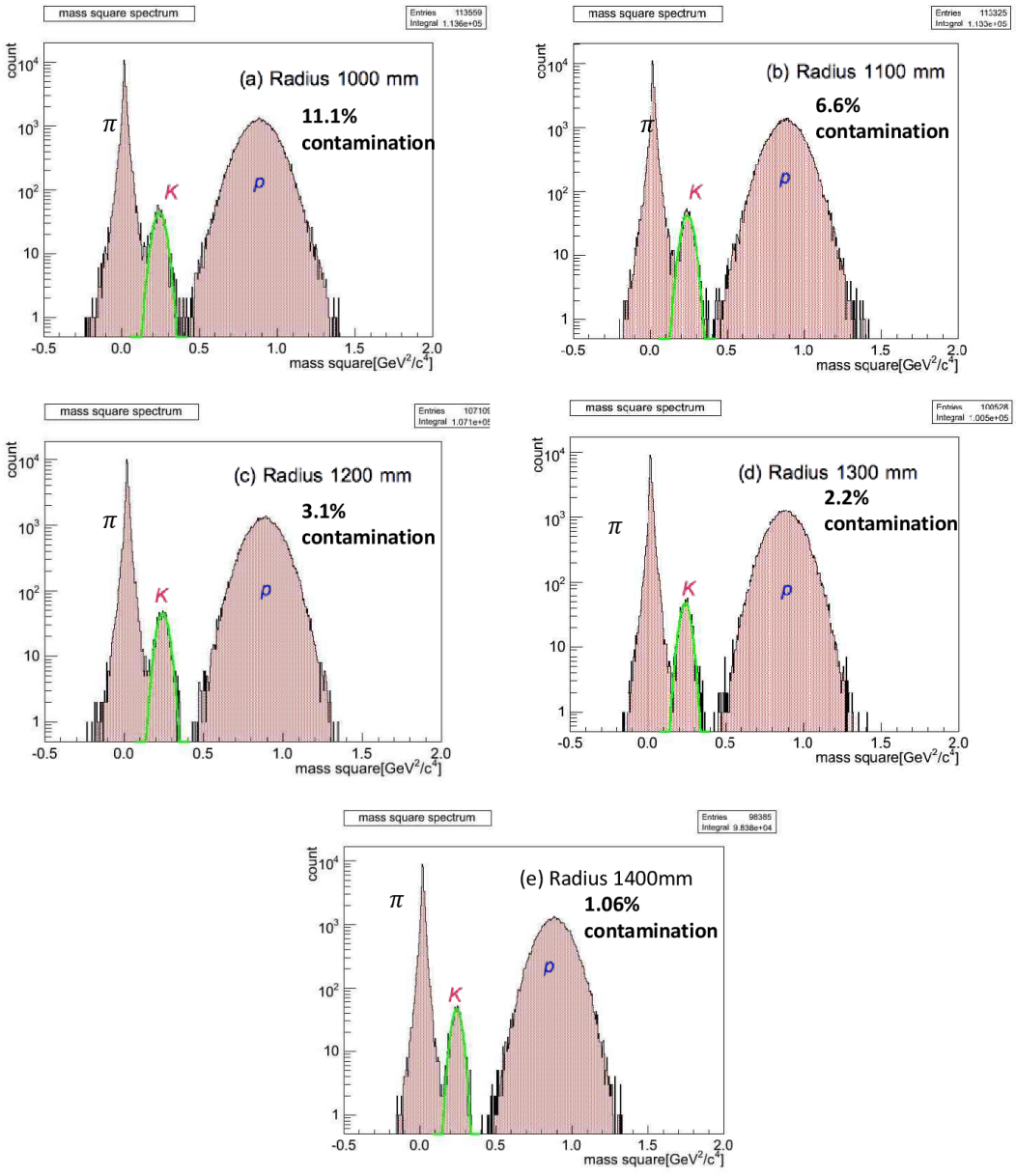

Figure 4.8: Mass square distributions for different MRPC position. The curve is a fit of gaussian for Kaon candidates.

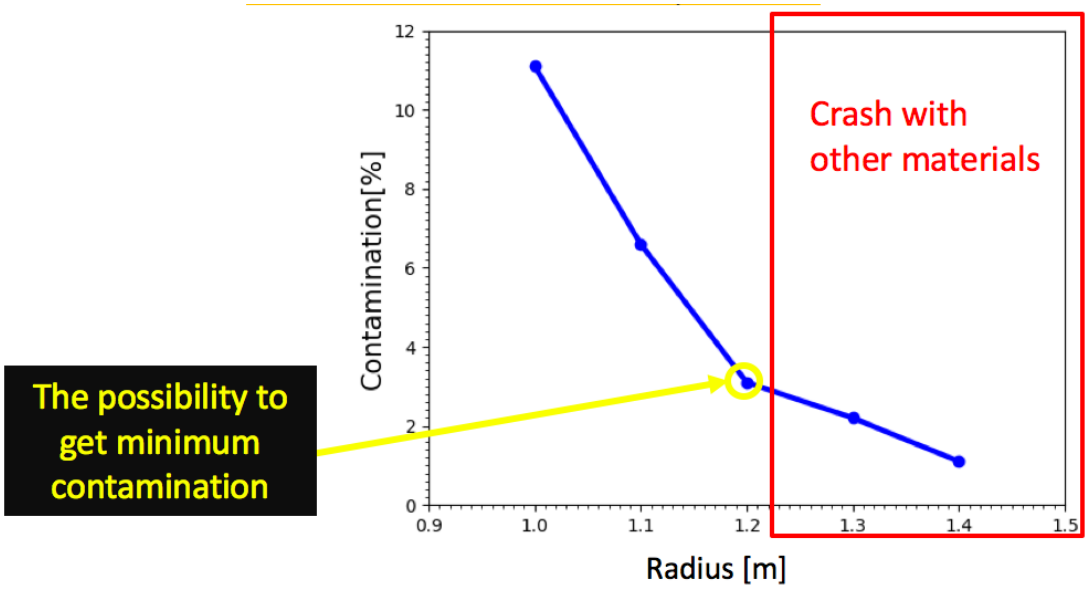

Figure 4.9: Contamination ratio dependency on the position

kind of spectrometers have the smaller acceptance. On the other hand, NKS2 can measure large kinematic coverage.

Note: For $K^+\Lambda$ coincidence event measurements, the geometrical acceptance is about 1% measurement.

4.3.3 Expected Missing Mass Spectrum

We can get information about missing mass spectrum by using conservation of energy,

$$E_\gamma + E_d = E_{K^+} + E_\Lambda n \tag{4.3.4}$$

The squared missing mass are calculated as follows,

$$M_{\Lambda n}{}^2 = (E_\gamma + E_d - E_{K^+})^2 - (\overrightarrow{p_\gamma} + \overrightarrow{p_d} - \overrightarrow{p_{K^+}})^2 \tag{4.3.5}$$

The missing mass distribution in the inclusive measurement of $\gamma d \to K^+\Lambda n$ reaction (Figure 4.11) are given in Figure 4.12. These distributions were obtained for photon energies of 800-1300 MeV.

The relative momentum in the $\Lambda - n$ system was calculated for each event, and an enhancement factor in the equation 2.1.2 was applied as a weight to the cross-section.

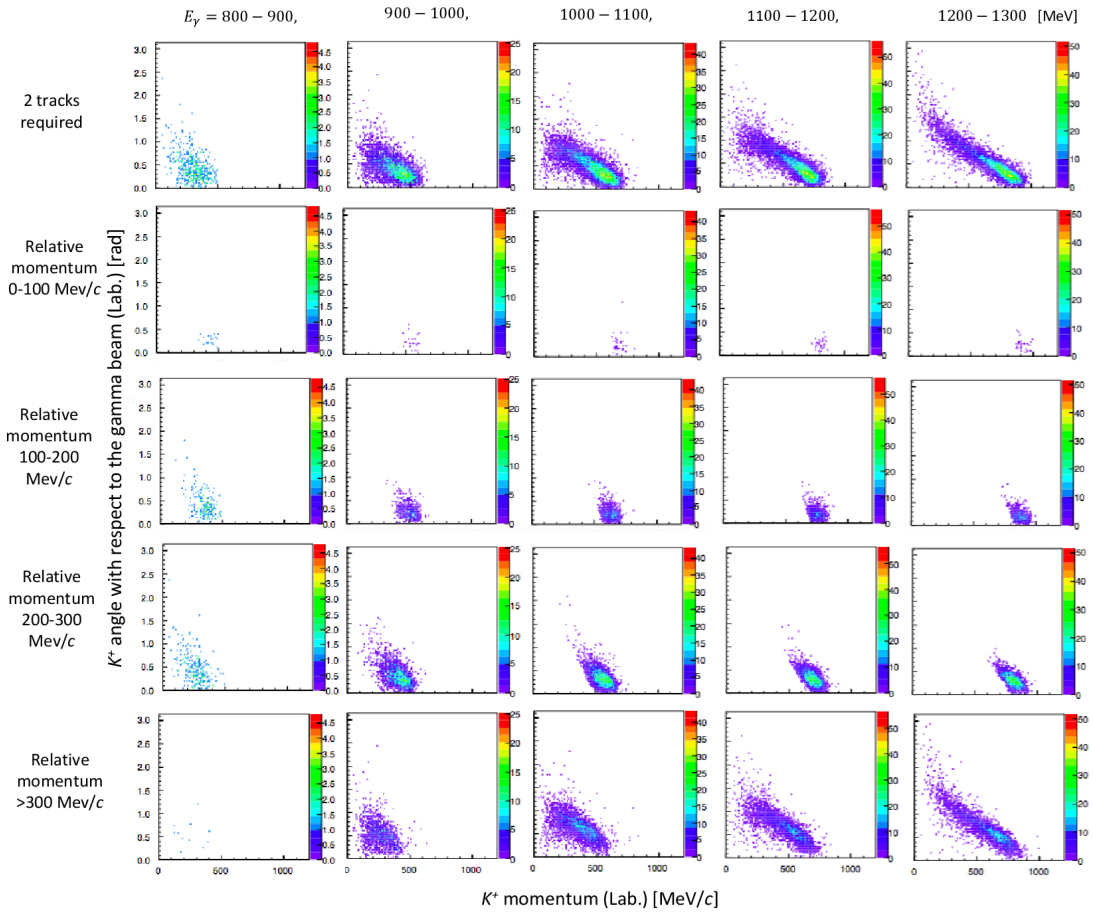

Figure 4.10: K^+ yield as a function of angle (0 to π rad) and momentum (0 to 1.2 GeV/c) in the laboratory frame.

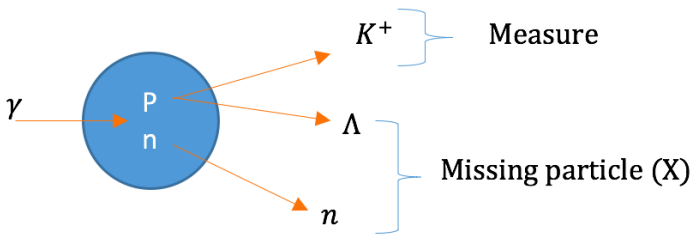

Figure 4.11: Reaction which we use in this experiment

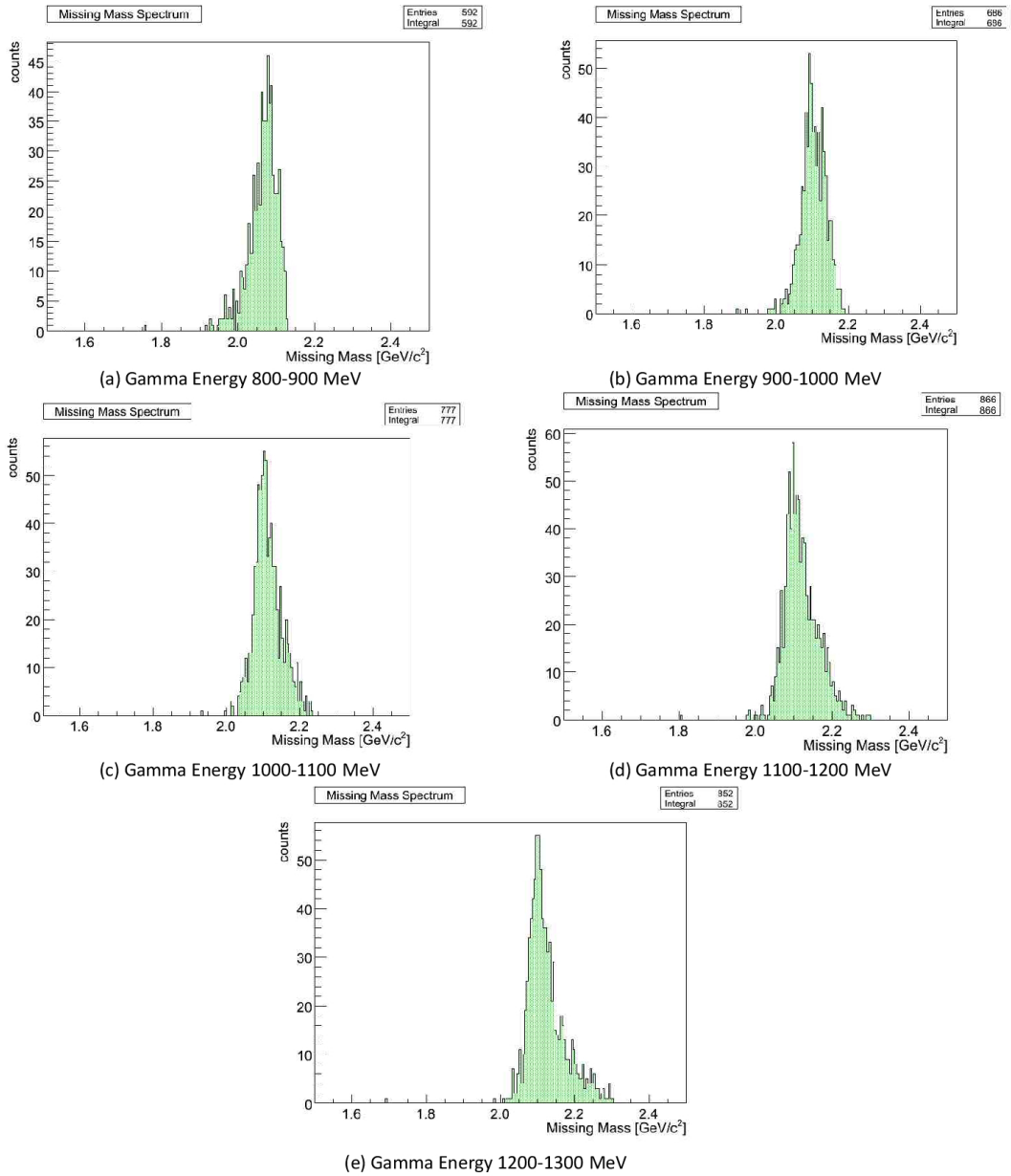

Figure 4.12: The K^+ yield as a function of the missing mass of $\Lambda - n$ calculated from K^+ momentum.

We requested that two charged particles pass through IH and MRPC in the simulation, which is the same requirement in the trigger in the experiment.

The top row histogram in Fig. 4.13 shows K^+ yield as a function of photon beam energy (E_γ). The second row histogram shows that the enhancement factors are greater in the lower (E_γ) regions (near the threshold) but still remain in the higher (E_γ) regions.

The bottom plot in Fig. 4.13 shows a relative error of the enhancement factors. The relative error is calculated by

$$\sqrt{f_e}/f_e \tag{4.3.6}$$

where f_e is the enhancement factors. Each plot contains of 4 model calculation. The S-wave singlet and triplet scattering length and effective range parameters are listed in table 4.1. Here the results from the Nijmegen model are denoted as $\mathrm{Nijm_D}$ [16]. The NSC parameters are taken from NSC89 [18] and NSC97 f [19]. The parameters given by J*ü*elich model denoted as $\mathrm{Jue_A}$ [20].

Model	a_s **(fm)**	r_s **(fm)**	a_t **(fm)**	r_t **(fm)**
Nijmegen D	-2.03	3.66	-1.84	3.32
NSC89	-2.86	2.91	-1.24	3.33
NSC97f	-2.68	3.07	-1.67	3.34
Jüelich A	-1.56	1.43	-1.59	3.16

Table 4.1: Potential model predictions of the S-wave singlet and triplet scattering length and effective range

The relative error of the enhancement factor indicates how a model can be distiguished from the others. We want to distinguish some models, because there are different $\Lambda-N$ potential between each models. If we can deside $\Lambda-N$ potential, we can understand about a part of nuclear physics including up, down, and strange quark. We found that 1% statistical error is required to distinguish the models (10000 counts of K^+) from Figure 4.14. Assuming triangle cross section, the necessary statistics is 30×10^3 K^+'s in E_γ=800-1100 MeV.

The Figure 4.15 are the K^+ yield as a function of missing mass of Λn calculated from K^+ momentum. Λn missing mass distributions for 5 different gamma energy ranges. The top left figure for E_γ=800-900 MeV, the top right figure for E_γ=900-1000 MeV, the middle left figure for E_γ= 1000-1100 MeV, the middle right figure for E_γ= 1100-1200 MeV, and the bottom left figure for E_γ= 1200-1300 MeV. It is clear that

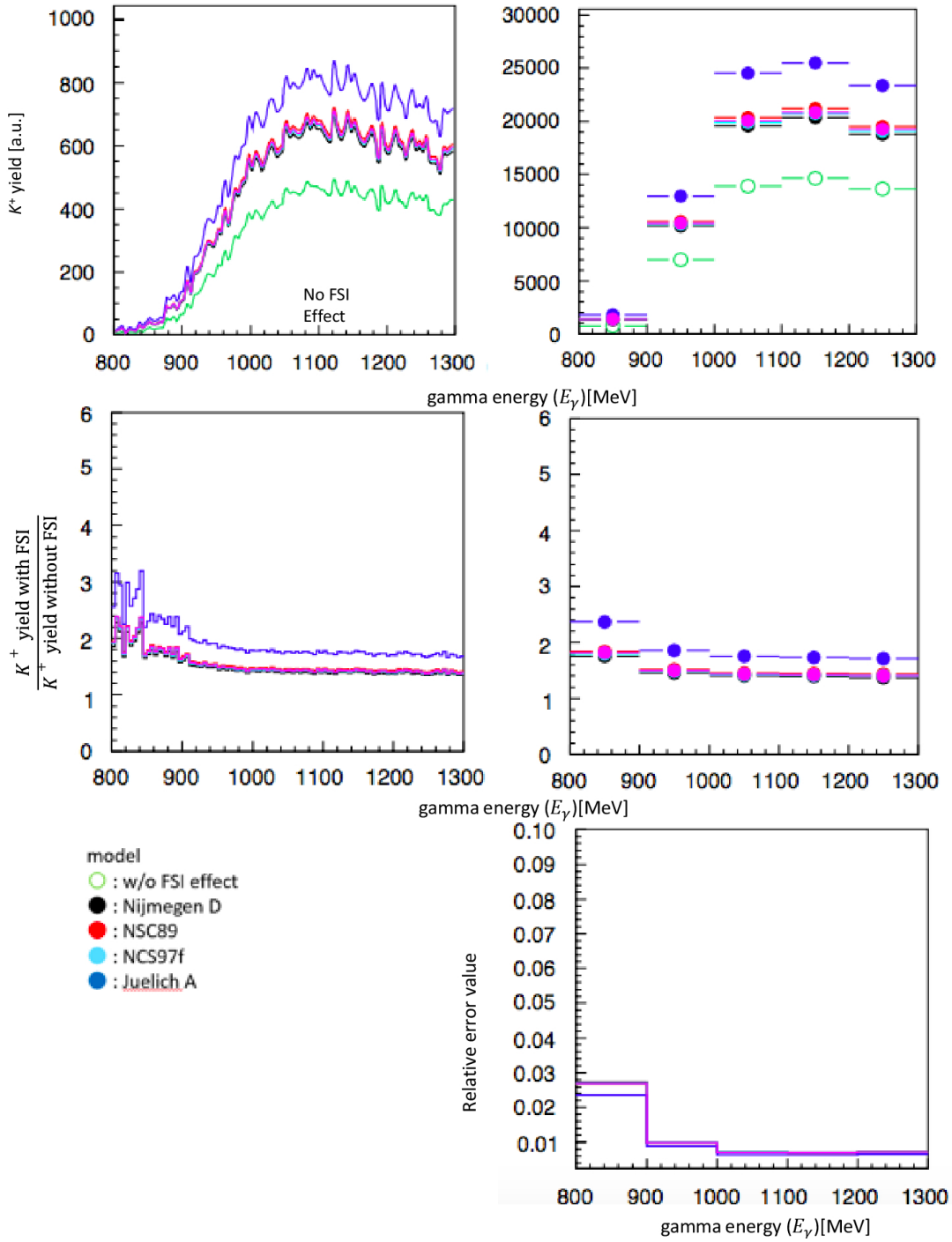

Figure 4.13: The top figures show number of K^+ event as a function of photon energy. The smallest yield plot is corresponding to no FSI effect and the others are included FSI effect from various potentials. The difference of left and right plots is bin width. The middle plots show the enhancement factor as a function of photon enegy. The middle-left and middle-right plots are corresponding to the top figures, respectively. The bottom plot shows the relative error values for each enhancement factor.

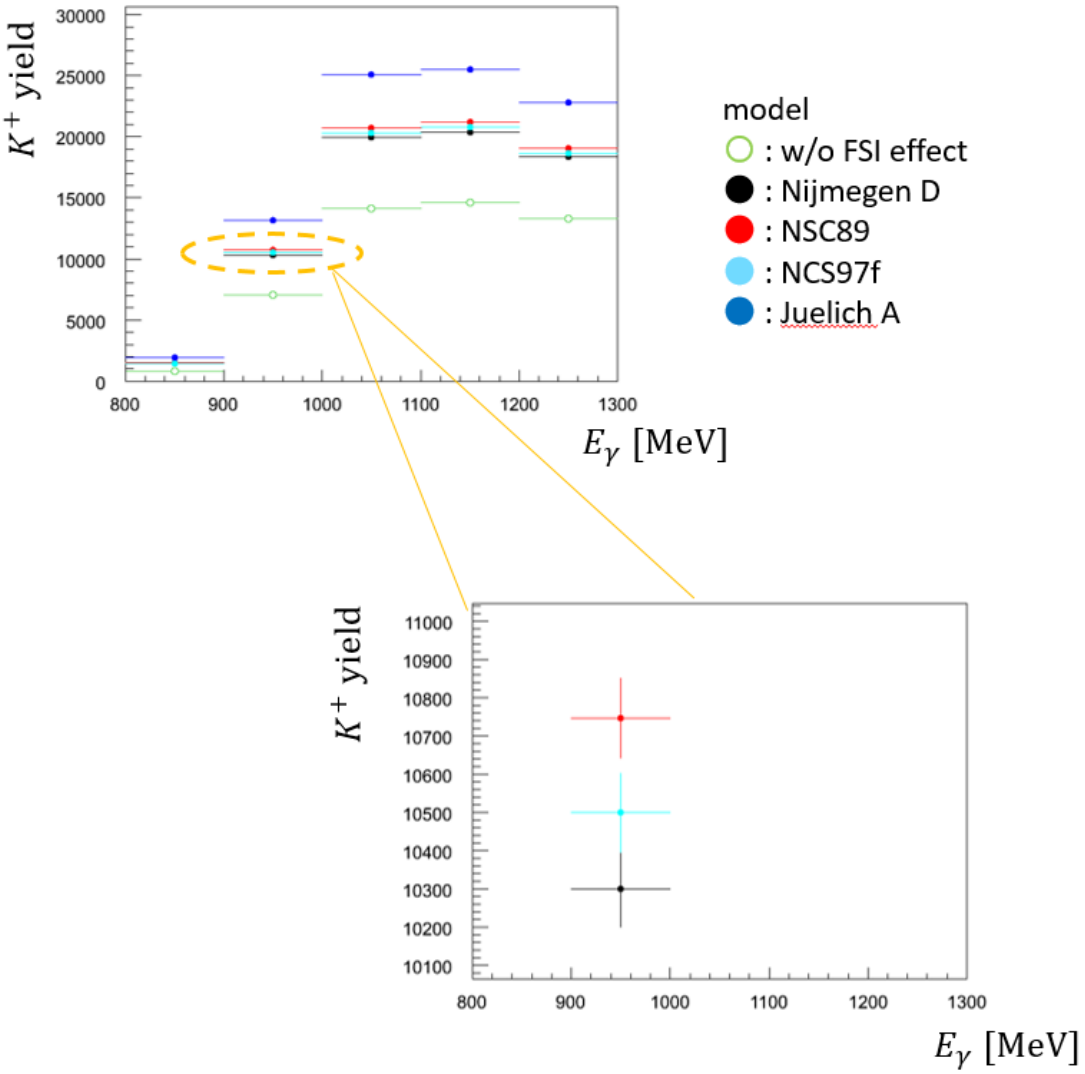

Figure 4.14: The number of K^+ as a function of photon energy (E_γ)

the yield was increased as a result of the FSI effect in not only in threshold region but also in E_γ=1200-1300 MeV

4.3.4 Beam Time Estimation

In the previous section, we showed that we need 10000 K^+ in the bin of E_γ = 800 - 1100 MeV. Assuming that requirement is the same over the all E_γ region of BM4 tagger (800 - 1100 MeV), that requirement became30×10^3 over all E_γ on Tagger.

The NKS2 experiment took 4.0×10^{12} tagged photon event for $\approx 700 K^0_S$ in 2006 - 2007 beam time [23]. It is corresponds to 83 shift of ELPH (1 shift is 12 hours).

The geometry acceptance for K^+ single measurement with 2-charged-particle trigger has been estimated as about 20% of all events by the GEANT4 simulation [5]. The K^0_S acceptance was about 1% order. Therefore, we expect about 20 times larger K^+ acceptance than K^0_S.

The number K^+ per shift will be

$$\frac{700(\text{number of} K^{0}{}_{S})}{83(\text{shift})} \times 20 = 168 \tag{4.3.7}$$

To obtain $30 \times 10^3 K^+$'s, we need 180 shifts (90 days).

NKS2 has a large acceptance ($\sim \pi$ sr), so we can detect K^+ with wider solid angle. On the other hand, from the view point of the yield of K^+, an experiment at Jefforson Lab (JLab) has more advantage than that NKS2 because of higher beam rate at Jlab. When we estimate a total cross section, we calculate differential cross section from experimental data, and integrate that for all solid angle. K^+ is detected by Kaon arm (HKS) at JLab, and Kaon arm is fixed at one angle for the electron beam line. Moreover, acceptance of Kaon arm is very small ($\sim$ 20 msr with splitter). So we can detect K^+ only limited solid angle, and this is disadvantage to calculate total cross section. So, from results of simulation, we can ensure that this experiment is feasible in the NKS2 .

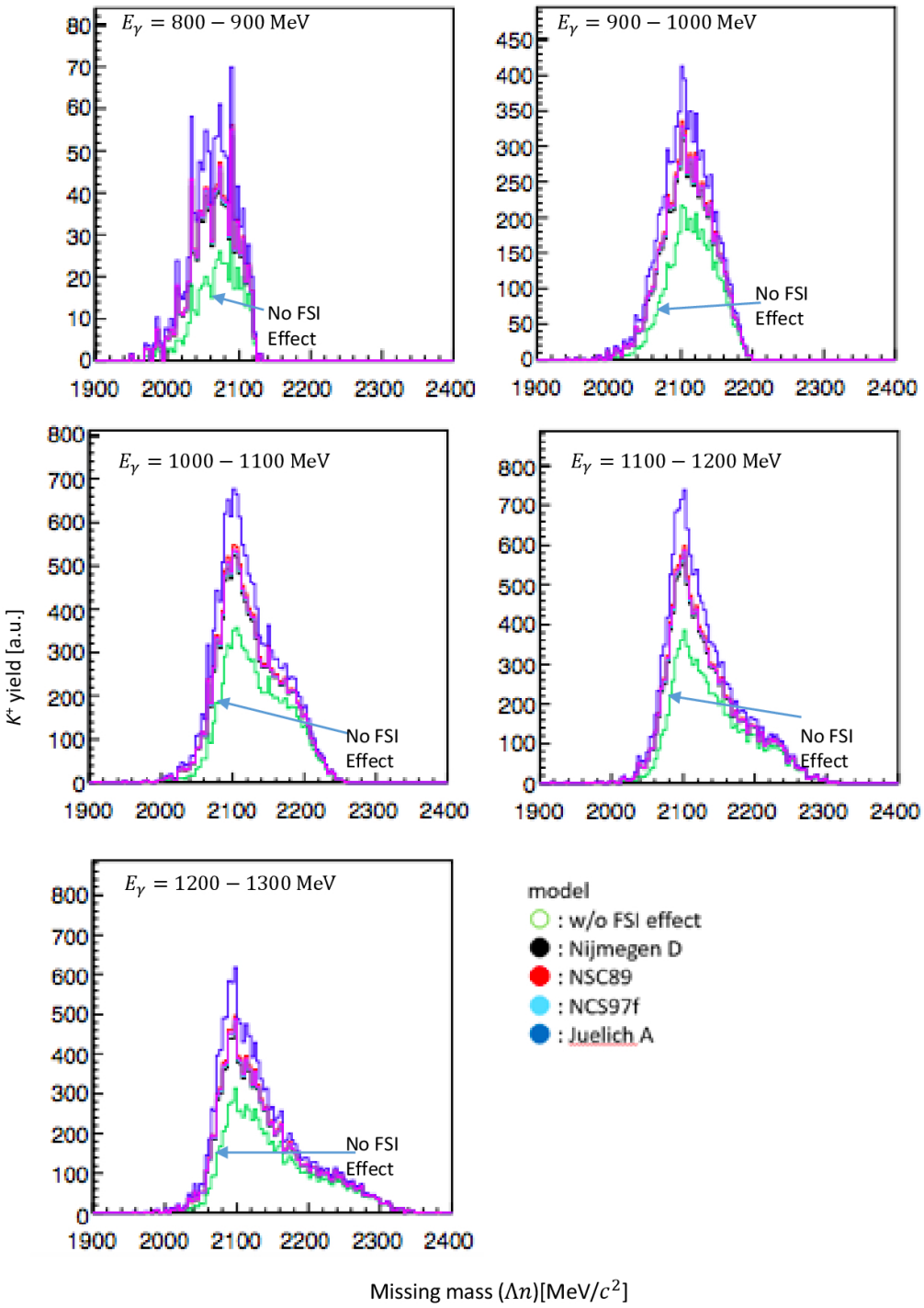

Figure 4.15: The K^+ yield as a function of the missing mass of $\Lambda - n$ calculated from K^+ momentum.

5

Summary

This thesis presented an upgrade plan for the Neutral Kaon Spectrometer 2 (NKS2), in which time resolution of hodoscopes are not enough to separate kaon, pion, and proton clearly at tthe present. A typical time resolution (σ) of hodoscopes was of the order of 400 ps, which was sufficient to separate pions and protons in a momentum range less than 800 MeV/c. We want to improve NKS2 Time-of-Flight resolution to separate kaon from other particles. By using Multi-gap Resistive Plate Chamber (MRPC), we expect that the NKS2 TOF resolution can be improved to less than 100 ps and can identify the $\gamma d \to K^+ \Lambda n$ reaction. To study the feasibility of the Λ-n Final State Interaction (FSI) in NKS2, I designed an experiment to study the Λ-n interaction via FSI with the GEANT4 simulation.

From mass squared distributions plots with a fit to a Gaussian function, the separation of pion, kaon, and protons is evident. It means we can detect Kaon because MRPC has a good time resolution of $\sigma \approx 100$ ps.

We can estimate the probability of multi hit by changing number of segment. From simulation results, we get the reasonable number of segmentation are around 202 to get 1.8 % probability of multi hit.

Radius parameter changes (Geometry Construction Acceptance) is refers to purely geometric fiducial volume of the detector. If the radius of detector are 1000 mm, 1100 mm, 1200 mm, 1300 mm, 1400 mm, so we get the acceptance are 1.40π sr, 1.29π sr, 1.19π sr, 1.10π sr, 1.03π sr, respectively. Acceptance will be larger if the radius of detector smaller. On the other hand, we do not set the radius of MRPC to small size, because mass resolution depend on beta and beta resolution. So, we should search best

point satisfying better acceptance and resolution. By applying cylindrical geometry, 1200 mm radius can optimize the value of acceptance.

Contamination depends of changing distance from the center (target position) to MRPC. Contamination of distance 1 m is 11.1 %, contamination of distance 1.1 m is 6.6 %, contamination of distance 1.2 m is 3.1 % (same as position of OH), contamination of distance 1.3 m is 2.2 %, contamination of distance 1.4 m is 1.06 %. 1.4 m will only have 1.06 % contamination. But, in NKS2 we have limit space for putting the cylinder detector inside the dipole magnet. So, the posibility to get minimum contamination is 1.2 m.

From the result, we can see the enhancement factors by Λn FSI effect are larger in lower E_γ region (800-900 MeV), but still remain higher region. It is clear that the yield was increased as a result of the FSI effect in wide region. The relative error of the enhancement factor indicates how a model can be distinguished from the others. We found that 1% statistic error is required to distinguish the models (10000 counts of K^+) . Assuming triangle cross section that indicates that $30 \times 10^3 K^+$'s in E_γ=800-1100 MeV.

The enhancement by Λn FSI effect is evident in low Λn relative momentum regions. The small angle (respect to gamma beam direction) region of K^+ in lab frame is corresponding to small Λn relative momentum region. It is due to Lorentz boost. In the low relative momentum region, events are located in the forward angle region of K^+ but not only at zero degree. It suggests that a wide coverage of the acceptance is necessary to measure the FSI enhancement effect, which can be measured by the NKS2.

The geometry acceptance for K^+ single measurement with 2-charged-particle trigger has been estimated about 20% for all events by the GEANT4 simulation. The K^0_S acceptance was about 1% order. The NKS2 experiment took 4.0×10^{12} tagged photon event for $\approx 700 K^0_S$ in 2006 - 2007 beam times. It is related to 83 shift of ELPH (1 shift is 12 hours). Using scaling of acceptance and data analyzed previously taken with NKS2, we predict that 180 shifts (90 days) are required to obtain $30 \times 10^3 K^+$'s to have 1% precision of the K^+ yield. It will allow us to discriminate models. So, from results of simulation, we can ensure that this experiment is feasible in the NKS2.

Bibliography

[1] K. Tsukada. *Photoproduction of Neutral Kaons on the liquid deuterium target in threshold region.* Phys Rev, C 78, 014001 (2008). iii, 13

[2] K. Tsukada. *Photoproduction of Neutral Kaons on the liquid deuterium target in threshold region.* Phys Rev, C 83, (039904(E) (2011). iii, 13

[3] K.M. Watson. *The Effect of Final State Interactions on Reaction Cross Sections.* Phys. Rev. 88, 1163 (1952). iv, 6, 9

[4] A.B. Migdal. *The Theory of Nuclear Reactions with Production of slow particles.* Sov, Phys. JETP 1, 2 (1955). iv, 6, 9

[5] M. Kaneta. *Study of* Λ*-n Interaction via FSI in* γ*-d Reaction.* HYP2015 (2016). v, 11, 12, 50

[6] E. Klempt. *Baryon spectroscopy.* Rev. Mod. Phys., 82:1095 (2010). 2

[7] B. Povh *et, al. Particle and Nuclei An Introduction to the Physical Concepts 5th Edition.* Springer (2006). 4, 5

[8] P. E. Shanahan. *Strangeness and Charge Symmetry Violation in Nucleon Structure.* Springer (2016). 5

[9] A. Esser, S. Nagao, F. Schulz, *etal* [A1 Collaboration]. *Observation of* ${}^{4}_{\Lambda}H$ *Hyperhydrogen by Decay-Pion Spectroscopy in Electron Scatteringy.* Phys. Rev. Lett. 114, 232501 (2015). 6

[10] S. P. Parker. *McGraw-Hill Dictionary of Scientific Technical Terms, 6E.* McGraw-Hill Companies, Inc (2003). 9

[11] L.B. Madsena *Effective range theory.* Institute of Physics and Astronomy, University of Aarhus, 8000A rhus C, Denmark (2002). 9

[12] H. Yamazaki *et, al. The 1.2 GeV photon tagging system (STB-Tagger) at LNS.* Research Report of Laboratory of Nuclear Science, 36:45-52 (2003). 14

[13] ATLAS *Amplifier-Shaper-Discriminator ICs and ASD Boards.* ATLAS International Note MUON NO. 1, October 1999. 22

[14] B. O. Beckford. *Study of the Strangeness Photoproduction Process in the $\gamma d \to \Lambda X$ Reaction at Photon Energies up to 1.08 GeV.* PhD thesis, Tohoku University, Sendai, Japan (2012). 33

[15] H. Yamamura *et, al. Inclusive K^+ and exclusive K^+Y photoproduction on the deuteron: $\Lambda-$ and $\Sigma-$ threshold phenomena.* Phys. Rev. C61, 014001 (1999). 42

[16] M. M. Nagels, T. A. Rijken, and J. J. de Swart. *Baryon-baryon scattering in a one-boson-exchange-potential approach. II. Hyperon-nucleon scattering.* Phys. Rev. D 20, 2547 (1977). 47

[17] M. M. Nagels, T. A. Rijken, and J. J. de Swart. *Baryon-baryon scattering in a one-boson-exchange-potential approach. III. A nucleon-nucleon and hyperon-nucleon analysis including contributions of a nonet of scalar mesons.* Phys. Rev. D 20, 1633 (1979).

[18] P. M. M. Maessen, Th. A. Rijken, and J. J. de Swart. *Soft-core baryon-baryon one-boson-exchange models. II. Hyperon-nucleon potential.* Phys. Rev. C 40, 2226 (1989). 47

[19] V. G. J. Stoks, Th. A. Rijken, and J. J. de Swart. *Soft-core baryon-baryon potentials for the complete baryon octet.* Phys. Rev. C 59, 3009 (1999). 47

[20] A. Reuber, K. Holinde, and J. Speth. *Meson-exchange hyperon-nucleon interactions in free scattering and nuclear matter.* Nucl. Phys. A570, 543 (1994). 47

[21] S.P. Verma, D.P. Sural. *Short Range Repulsion In Hypernuclei And Calculation Using K Harmonics.* Phys.Rev. C22, 229 (1980)

[22] R.K. Bhaduri, Y. Nogami, and W.van DIjk. *Analysis of the $\Lambda - N$ Interaction.* Phys.Rev. 155, 1671 (1967)

[23] K. Futatsukawa. *An investigation of the elementary photoproduction of strangeness in the threshold region.* PhD thesis, Tohoku University, Sendai, Japan (2011). 50